University of Stavanger

Faculty of Science and Technology

MASTER'S THESIS

Study program/Specialization: Petroleum Engineering / Drilling and Well Engineering	Spring semester, 2017 Open / ~~Restricted access~~
Writer: **Kristoffer Wareberg**	..... (Writer's signature)

Faculty supervisor: **Mesfin Agonafir Belayneh**

External supervisor(s):

Thesis title:

Dynamic Simulation Study on Alternative Marine Drilling Riser Materials in the Deep-Waters of the Norwegian Sea

Credits (ECTS): 30

Key words: - Marine Drilling Riser - Alternative materials - Aluminum, titanium - The Norwegian Sea - Aasta Hansteen - OrcaFlex	Pages: 72 + enclosure: 32 Stavanger, 15/06-2017 Date/year

Frontpage for master's thesis
Faculty of Science and Technology
Decision made by the Dean October 30th 2009

Dynamic Simulation Study on Alternative Marine Drilling Riser Materials in the Deep-Waters of the Norwegian Sea

Kristoffer Wareberg

Faculty of Science and Technology
University of Stavanger

This thesis is submitted for the degree of
Master of Science

June 2017

Acknowledgements

This thesis was written as part of completing a five-year Master degree in Petroleum Engineering at the University of Stavanger. In that regard, I would like to thank my scientific supervisor Mesfin Agonafir Belayneh, at The Department of Pertroleum Engineering at the University of Stavanger. His office door was always open whenever I had questions about my research or just needed to be motivated. I would also like to thank Einar Nygaard in Statoil for providing me with valuable environmental data.

My loving girlfriend Vibeke deserves a big thanks. She have been my "blow out preventer" and encouraged me throughout this semester. Finally, thanks to all my fellow students in Petroleum Engineering at the University of Stavanger. We've shared so many good times together, and without them the studies would never been that interesting and gratifying. Thank you!

Kristoffer Wareberg

Stavanger 2017

Abstract

In the pursuit of more oil and gas to meet the growing demand and replace the declining production, the offshore industry is pushed to invest, explore and drill new wells in deeper waters with harsh environments and with a possibility of HPHT wells and sour well flows. Drilling risers with strength and corrosion resistance capable of handling these extreme conditions are accordingly required. As the water depth increases, the length and weight of the riser might lead to problems in terms of; increased loadings on the handling equipment and tensioner system, as well as storage and transportation limitations. Today, the conventional riser material is steel. Steel is a strong and relatively cheap material. However, it is heavy and not very corrosion resistant. Hence, the industry has turned its focus to lighter alternative materials. Aluminum and titanium risers with their light weight, high strength-to-weight ratio and good corrosion resistance are potential candidates to substitute the heavy steel risers.

In order to assess aluminum and titanium as alternative materials in riser design and determine if they are suitable for operations in the harsh environment in the Norwegian Sea, simulation studies in OrcaFlex has been conducted. The environmental data used in the simulations are from the Aasta Hansteen gas field, in an area of the Norwegian Sea where the water depth is about 1200 m. The output from the simulation software are compared with the ISO standard 13624 to find the maximum flex joint angles and von Mises stress.

The results from the dynamic simulations show that wave height and drilling fluid density influences the effective tension, flex joint angles and the von Mises stress. The applied top tension proves to have the biggest impact on the results, and should be closely considered during the design phase.

Aluminum and titanium both proves to fulfill the given design parameters, and can potentially be an alternative to the conventional steel riser in drilling operations in the Norwegian Sea. However, long term properties such as fatigue and corrosion should be investigated to get the full understanding.

Table of contents

List of figures **xiii**

List of tables **xvii**

Nomenclature **xix**

1 Introduction **1**
1.1 Research Motivation and Problem Statement 2
1.2 Objectives 3
1.3 Structure of Thesis 4

2 The Marine Drilling Riser **5**
2.1 Main Components 5
2.1.1 Motion-Compensating Equipment 7
2.1.2 Flex Joints 8
2.1.3 Buoyancy Modules 8
2.1.4 Lower Marine Riser Package (LMRP) 9
2.2 Application of Alternative Materials 10
2.2.1 Aluminum Riser 10
2.2.2 Titanium Riser 11
2.3 Standards and Regulations 11
2.3.1 API RP 16Q 11
2.3.2 ISO 13624 14

3 Fundamentals of Riser Mechanics and Hydrodynamic Loads **15**
3.1 Riser Mechanics 15
3.1.1 Effective Tension 15
3.1.2 Principal Stresses 19
3.1.3 Von Mises Failure Criterion 21

3.2 Hydrodynamic Loads . . . 22
3.2.1 Waves . . . 22
3.2.2 Currents . . . 23
3.2.3 Vortex Induced Vibrations (VIV) . . . 24
3.2.4 Morison Equation . . . 24

4 Simulation Study **27**
4.1 The Norwegian Sea: Aasta Hansteen field . . . 27
4.1.1 Wind . . . 29
4.1.2 Waves . . . 30
4.1.3 Currents . . . 32
4.2 OrcaFlex . . . 33
4.2.1 Coordinate System . . . 33
4.2.2 Marine Drilling Riser Structural Model . . . 33
4.2.3 Modelling of Environmental Loading . . . 37
4.2.4 Static Analysis and Dynamic Analysis . . . 40

5 Dynamic Simulation Results **41**
5.1 Minimum Effective Tension . . . 42
5.1.1 Steel Riser . . . 43
5.1.2 Aluminum Riser . . . 44
5.1.3 Titanium Riser . . . 45
5.2 Minimum Effective Top Tension . . . 46
5.2.1 Steel Riser . . . 47
5.2.2 Aluminum Riser . . . 48
5.2.3 Titanium Riser . . . 49
5.3 Maximum Upper Flex Joint Angles . . . 50
5.3.1 Steel Riser . . . 51
5.3.2 Aluminum Riser . . . 52
5.3.3 Titanium Riser . . . 53
5.4 Maximum Lower Flex Joint Angles . . . 54
5.4.1 Steel Riser . . . 55
5.4.2 Aluminum Riser . . . 56
5.4.3 Titanium Riser . . . 57
5.5 Maximum von Mises Stress . . . 58
5.5.1 Steel Riser . . . 59
5.5.2 Aluminum Riser . . . 60

5.5.3 Titanium Riser 61

6 Summary and Discussion **63**
6.1 Effect of Wave Height 63
6.2 Effect of Drilling Fluid Density 64
6.3 Effect of Applied Top Tension 65
6.4 Application of Alternative Materials 67

7 Conclusion **69**
7.1 Concluding remarks 69
7.2 Suggestions for future work 70

References **71**

Appendix A **73**
A.1 Maximum Effective Tension 73
A.2 Input and Calculations of Minimum Required Top Tension 76
A.3 Maximum upper and lower flex joint angles 79
A.4 Maximum von Mises Stress 80
A.5 Maximum Bending Stress 81
A.6 Maximum Axial Stress 82

List of figures

1.1 Overview of the riser system [6] 2

2.1 Complete Riser Joint [24]. 6
2.2 Key Components in a Drilling Riser System [24] 7
2.3 Direct Acting Tensioner System [22] 8
2.4 A Typical Drilling Riser system with upper and lower flex joints [9] . . 9

3.1 Archimedes' law by superposition [19] 16
3.2 Internal forces acting on a submerged body segment [19] 17
3.3 Pipe with internal and external fluids and the equivalent force system [19] 18
3.4 In-wall Stresses [19] 19
3.5 The stress distribution in a thick-walled cylinder when $P_a > P_b$ [5] . . . 20
3.6 Regular traveling wave characteristics [7] 23

4.1 Map showing the position of Aasta Hansteen Field in the Norwegian Sea [14] 28
4.2 All-year wind rose for the Aasta Hansteen Field for the period 1958-2008 [21] 29
4.3 All-year wave rose for the Aasta Hansteen Field for the period 1958-2008 [21] 30
4.4 OrcaFlex Coordinate System [16] 34
4.5 Schematic Diagram of the Drilling Riser System 34
4.6 Drilling vessel in OrcaFlex 35
4.7 OrcaFlex line model [16] 36
4.8 Current Velocity Distribution 38

5.1 Min. Effective tension at seabed, steel, drilling fluid density = $1025 kg/m^3$ 43
5.2 Min. Effective tension at seabed, steel, drilling fluid density = $1500 kg/m^3$ 43

5.3 Min. Effective tension at seabed, aluminum, drilling fluid density = $1025kg/m^3$ 44
5.4 Min. Effective tension at seabed, aluminum, drilling fluid density = $1500kg/m^3$ 44
5.5 Min. Effective tension at seabed, titanium, drilling fluid density = $1025kg/m^3$ 45
5.6 Min. Effective tension at seabed, titanium, drilling fluid density = $1500kg/m^3$ 45
5.7 Min. Effective top tension, steel, drilling fluid density = $1025kg/m^3$ . . 47
5.8 Min. Effective top tension, steel, drilling fluid density = $1500kg/m^3$ . . 47
5.9 Min. Effective top tension, aluminum, drilling fluid density = $1025kg/m^3$ 48
5.10 Min. Effective top tension, aluminum, drilling fluid density = $1500kg/m^3$ 48
5.11 Min. Effective top tension, titanium, drilling fluid density = $1025kg/m^3$ 49
5.12 Min. Effective top tension, titanium, drilling fluid density = $1500kg/m^3$ 49
5.13 Max. Upper flex joint angles, steel, drilling fluid density = $1025kg/m^3$ 51
5.14 Max. Upper flex joint angles, steel, drilling fluid density = $1500kg/m^3$ 51
5.15 Max. Upper flex joint angles, aluminum, drilling fluid density = $1025kg/m^3$ 52
5.16 Max. Upper flex joint angles, aluminum, drilling fluid density = $1500kg/m^3$ 52
5.17 Max. Upper flex joint angles, titanium, drilling fluid density = $1025kg/m^3$ 53
5.18 Max. Upper flex joint angles, titanium, drilling fluid density = $1500kg/m^3$ 53
5.19 Max. Lower flex joint angles, steel, drilling fluid density = $1025kg/m^3$. 55
5.20 Max. Lower flex joint angles, steel, drilling fluid density = $1500kg/m^3$. 55
5.21 Max. Lower flex joint angles, aluminum, drilling fluid density = $1025kg/m^3$ 56
5.22 Max. Lower flex joint angles, aluminum, drilling fluid density = $1500kg/m^3$ 56
5.23 Max. Lower flex joint angles, titanium, drilling fluid density = $1025kg/m^3$ 57
5.24 Max. Lower flex joint angles, titanium, drilling fluid density = $1500kg/m^3$ 57
5.25 Max. von Mises stress, steel, drilling fluid density = $1025kg/m^3$ 59
5.26 Max. von Mises stress, steel, drilling fluid density = $1500kg/m^3$ 59
5.27 Max. von Mises stress, aluminum, drilling fluid density = $1025kg/m^3$. 60
5.28 Max. von Mises stress, aluminum, drilling fluid density = $1500kg/m^3$. 60
5.29 Max. von Mises stress, titanium, drilling fluid density = $1025kg/m^3$ . . 61
5.30 Max. von Mises stress, titanium, drilling fluid density = $1500kg/m^3$ . . 61

6.1 Min. required applied top tension, drilling fluid density = $1500kg/m^3$. 67

A.1 Max. Effective tension in steel riser 73
A.2 Max. Effective tension in aluminum riser 73

A.3 Max. Effective tension in titanium riser 74
A.4 Max. Effective tension at seabed in steel riser 74
A.5 Max. Effective tension at seabed in aluminum riser 74
A.6 Max. Effective tension at seabed in titanium riser 75
A.7 Max. upper flex jt. angle for various design waves 79
A.8 Max. lower flex jt. angle for various design waves 79
A.9 Max. von Mises stress, drilling fluid density = $1500kg/m^3$ 80
A.10 Max. Bending stress, drilling fluid density = $1500kg/m^3$ 81
A.11 Max.Bending stress through the entire length of riser, drilling fluid density = $1500kg/m^3$ 81
A.12 Max. Axial stress, drilling fluid density = $1500kg/m^3$ 82
A.13 Max.Axial stress through the entire length of riser, drilling fluid density = $1500kg/m^3$ 82

List of tables

2.1 Max. Operating and Design Guidelines from API RP 16Q [2] 13
2.2 Max. Operating and Design Guidelines from ISO 13624-1:2009 [11] . . 14

4.1 Annual probability for extreme wind speed [21] 29
4.2 Spectral peak period T_p as a function of significant wave height H_s at the Aasta Hansteen Field [21] 31
4.3 Extreme significant wave heights and corresponding spectral peak periods [21] 31
4.4 Max. and mean currents speeds measured at the Aasta Hansteen field . 32
4.5 Structural Configuration of Drilling Riser 36
4.6 Riser Material Properties 37
4.7 Design Wave heights and periods 39

5.1 Minimum top tension determined by Eq. 2.1 46
5.2 Yield and allowable stress 58

6.1 Max. and Min. Tension boundaries 66

A.1 Distances 76
A.2 Constants 76
A.3 Riser Data 77
A.4 Auxilary Lines Data 77
A.5 Output 78

Nomenclature

Symbols

δ_s	Element length
Ψ	Angle with vertical
ρ	Fluid density
A_e	Cross-sectional area of section
A_{csaa}	Cross sectional area auxilary lines
A_{csar}	Cross sectional area riser
B_n	Net lift of buoyancy material
D	Outside diameter
d_r	Material density
d_w	Sea water density
dm	Drilling fluid density
f_D	Drag force
f_H	Hydrodynamic force
f_I	Inertia force
f_{wt}	Submerged weight tolerance factor
H_m	Drilling fluid column to point of consideration
H_s	Significant wave height

H_w	Sea water column to point of consideration
$H_{LMRP+BOP}$	Height of LMRP + BOP
H_{RKB-ML}	Distance from RKB to mud line
$H_{RKB-MSL}$	Distance from RKB to MSL
H_{SS+T}	Height of storm surge + tide
H_{TR-MSL}	Distance from tensioner ring to MSL
H_{WH}	Height of wellhead
ID	Inner diameter
ID_a	Inner diameter auxilary lines
ID_r	Inner diameter riser
L_r	Riser Length
L_{rsub}	Submerged riser length
M	Moment
N	Number of tensioners
n	Number of tensioners subject to sudden failure
OD	Outer diameter
OD_a	Outer diameter auxilary lines
OD_r	Outer diameter riser
P_a	Internal pressure
P_b	External pressure
p_e	Pressure in external fluid
R_f	Reduction factor
T	Tension
t	Wall thickness

T_e	Effective tension
T_{min}	Minimum required top tension
T_{SRmin}	Minimum slip ring tension
T_{true}	True tension
T_{tw}	True wall tension
V	Volume of fluid
W_a	Apparent weight
W_f	Weight of displaced fluid
W_s	Submerged riser weight
W_t	True weight

Abbreviations

API	American Petroleum Institute
asb	Above sea bottom
BOP	Blow Out Preventer
DNV	Det Norske Veritas
DTL	Dynamic Tension Limit
EDP	Emergency Disconnect Package
HPHT	High-Pressure High-Temperature
ISO	International Organization of Standardization
LFJ	Lower Flex Joint
LMRP	Lower Marine Riser Package
ML	Mud Line
MSL	Mean Sea Level
N/A	Not Applicable

NCS	The Norwegian Continental Shelf
RAO	Response Amplitude Operators
RKB	Rotary Kelly Bushing
SAF	Stress Amplification Factors
VIV	Vortex Induced Vibrations
WH	Wellhead
WOB	Weight On Bit

Chapter 1

Introduction

According to the World Energy Outlook the era of fossil fuels appears far from over, and the global oil demand continuous to grow until 2040 [10]. Investment and new discoveries is necessary to meet this growing demand and replace declining production. This means that it is important to maintain the exploration activity at a high level. It is reasonable to claim that the most accessible and least technically challenging fields are already found, this forces the exploration companies to drill in more and more hostile places and in deep- and ultra deep-waters.

It's not just the environment that gets harsher, the reservoirs also become more extreme with high-pressure and –temperature wells (HPHT wells) and sour well flows. The combination of deep-water drilling and aggressive wells leads to higher demands in terms of offshore equipment weight, strength and corrosion resistance. The marine drilling riser is certainly the heaviest item used in drilling operations, and as it extends from the surface to seabed and serve as a conduit for drilling and well fluids it is highly exposed to hydrodynamic loads and corrosion. Hence, the industry has its focus on how to reduce the weight of the riser without it being at the expense of safety.

This thesis presents a simulation-based study of the loadings the mariner drilling riser is exposed to in regards the environmental conditions in the deep water areas of the Norwegian Sea. Dynamic simulations are performed in OrcaFlex, a well known analysis software for offshore marine systems. Steel, aluminum and titanium have all been used as riser materials throughout the simulations, the results are discussed and compared to each other.

1.1 Research Motivation and Problem Statement

The marine drilling riser is the connection between the subsea well and surface during drilling. It consists of several joints bolted together, forming a conduit for drilling fluids and equipment. The riser is exposed to great forces arising from vessel movement, hydrodynamic loads, pressure differences and applied tension, see Fig. 1.1.

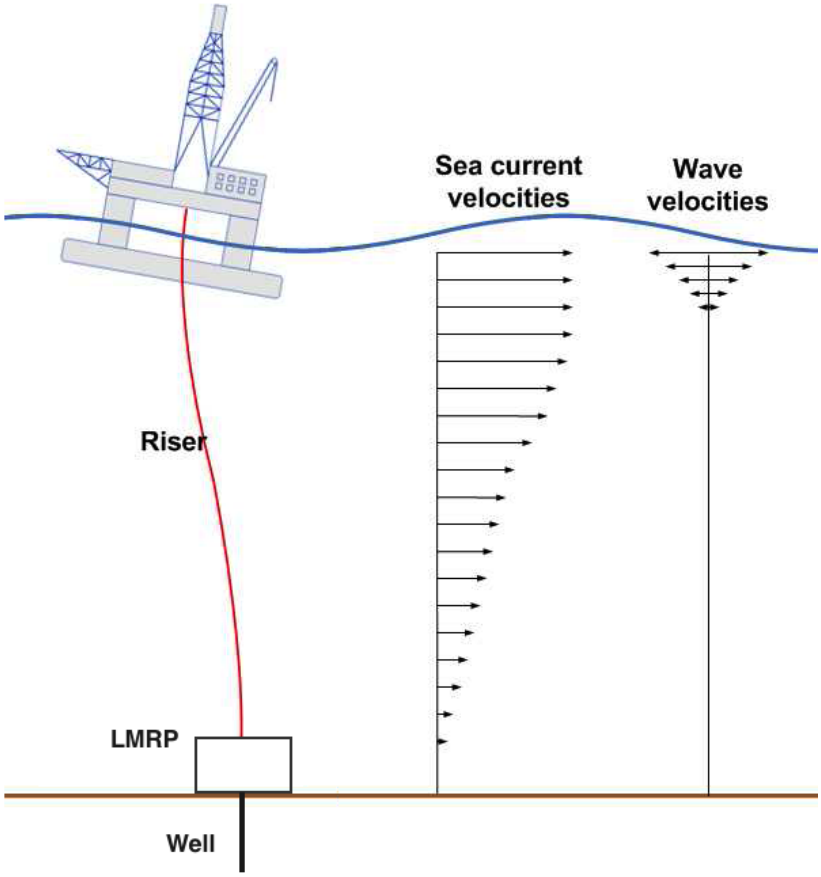

Fig. 1.1. Overview of the riser system [6]

As the water depth increases the physical and functional demands on the marine drilling risers system increases as well. The additional weight, space and loadings arising from increased water depth leads to higher demands on the drilling rig, equipment and the material properties. Alternative lighter materials, such as aluminum and titanium, can help reduce the weight, moderate the loadings associated with deep water drilling and possibly reduce the total lifetime costs.

The Norwegian Sea is known for its harsh environment. The large depths, big waves and high winds pose significant technical challenges for petroleum exploration and production. The area is considered a good candidate to base a simulation study on, when the purpose of the analysis is to address possible challenges in harsh deep water environments. The environmental data in this thesis is from the Aasta Hansteen gas field, located in the Norwegian Sea at a water depth of 1200 m.

In order to investigate if lighter materials actually can be an alternative to steel in the extreme environment and deep-waters of the Norwegian Sea, the following areas of concern need to be addressed:

- The effect wave heights, different drilling fluid densities and applied top tension have on effective tension, flex joint angles and von Mises stress.
- Will the alternative material properties fulfill the given design parameters and be able to operate in a safe manner in the Norwegian Sea.

1.2 Objectives

The main objective with this thesis is to assess the addressed problem areas presented above, in terms of:

- Get an understanding of the fundamental mechanics of the riser and the associated hydrodynamic loads.
- Evaluate the the extreme weather in the Norwegian Sea to get the correct simulation input.
- Perform riser simulation study in order to assess the effect wave heights, different drilling fluid densities and applied top tension have on the effective stresses, flex joint angles and von Mises stresses.
- Assess opportunities and challenges associated with application of aluminum and titanium risers as a substitute to the conventional steel riser in the Norwegian Sea.

This thesis is limited to a simulation study of steel, aluminum and titanium marine drilling risers, operating in the Norwegian Sea.

1.3 Structure of Thesis

This thesis is divided into seven chapters, the next chapter, Chapter 2 describes the marine drilling riser system and its main components, it also introduces alternative materials and presents standards with recommended practices.

Chapter 3 aims to explain the way the mariner drilling riser behave in the influence of hydrodynamic loads, beginning with the fundamental mechanics.

Chapter 4 presents the environmental conditions, it briefly explains the simulation software Orcaflex, and describes the build-up of the simulation model.

Chapter 5 presents the results from the dynamic simulation.

Chapter 6 summarizes and discusses the results from the previous chapter.

Chapter 7 presents the concluding remarks and recommendations for future work.

Chapter 2

The Marine Drilling Riser

Most offshore drilling operations are carried out using a marine drilling riser connected to a dynamically positioned floating drilling rig. The marine drilling riser provides communication between the subsea wellhead and surface by serving as a conduit for drilling fluid and cutting returns. In addition the riser enables transfer of equipment and drill string without interaction with the sea. The drilling fluid carried by the riser balances the pore pressure and is, in addition to the Blow Out Preventer (BOP), a primary barrier. Maintaining well control during drilling is the main concern for the operator. Hence, the marine drilling riser integrity is very important.

This chapter presents the most essential parts of the marine drilling riser system, alternative riser materials, and two standards, which includes a recommended practice for design.

2.1 Main Components

The marine drilling riser consists of a large diameter main tube with smaller external auxiliary lines clamped to it. The main tube is open to atmospheric pressure at the top end, therefore it does not have to be designed to withstand full well pressure. The auxiliary lines on the other hand are high pressure kill and choke lines used in the event of a gas kick, as well as booster and hydraulic lines used to inject fluid and provide power to the BOP. A typical drilling riser is made up by tubular joints in the range of 30- to 75-ft (9- to 23-meters) with a main tube diameter of 21". The joints are bolted together with connectors at the ends. Fig. 2.1 shows a drilling riser joint equipped with peripheral lines and end connectors [19].

The drilling riser system varies by company standards, drilling rig and design. However, in addition to the aforementioned riser joints a typical system consists of pup

joints, spider, gimbal, slip joint, motion-compensating equipment, flex joints, buoyancy modules and lower marine riser package (LMRP). The last four are described in more detail in the following section. While the rest are briefly presented below and in figure Fig. 2.2 [24].

Pup joints: The pup joints are smaller riser joints used to ensure a proper space-out for the riser.
Spider: The spider is located on the drill floor in the rotary table. The device is hydraulically actuated, and uses retractable jaws to support the weight and to maintain the stability of the riser during deployment and retrieval.
Gimbal: The gimbal is situated between the spider and the rotary table. Its function is to reduce shock and bending moments and equally distribute loads caused by the vessels roll/pitch motions, and allow the riser to rotate about the horizontal axis.
Slip joint: The slip joint is located below the gimbal, it consists of two concentric pipes that telescopes in and out, as the vessel heaves, to prevent or reduce destructive loads in the riser.

Fig. 2.1. Complete Riser Joint [24].

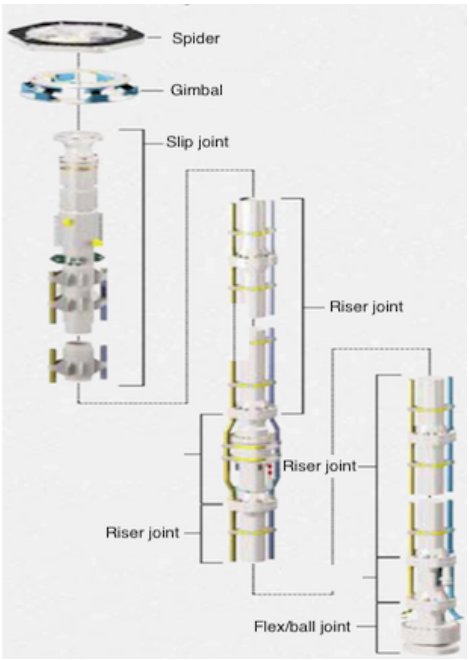

Fig. 2.2. Key Components in a Drilling Riser System [24]

2.1.1 Motion-Compensating Equipment

Floating drilling vessels move up and down and back and forth in response to the waves, wind and currents. To compensate for the motion and heave of the vessel, motion-compensating equipment are installed and function as the flexible link between the force of the ocean and the vessel. A typical motion-compensating system consists of riser tensioners, drill string compensator, and guideline and podline tensioners. Fig. 2.3 shows a direct acting tensioner system [2, 24].

Riser tensioners: The riser tensioners exists in multiple different designs and techniques. A typical tensioner uses hydraulic cylinders, connected to a number of high pressure gas accumulators, to maintain a near constant tension on the lines, which may be wire rope or chain. The lines are at one end attached to the tensioner, while the other end is secured by the tension ring on the outer barrel of the slip joint. The main purpose with the tensioners are to apply a continuous axial force to the riser, keeping it in tension to avoid buckling and collapse.
Drill string compensator: During drilling the driller relies on a constant and controllable weight on bit, to achieve such when the rig heaves a drill string compensator is located between the traveling block and rotary table.
Guideline and podline tensioners: Guideline wire ropes and the wire ropes that

support the BOP control podlines as the rig heaves, are kept in constant tension by the guideline and podline tensioner.

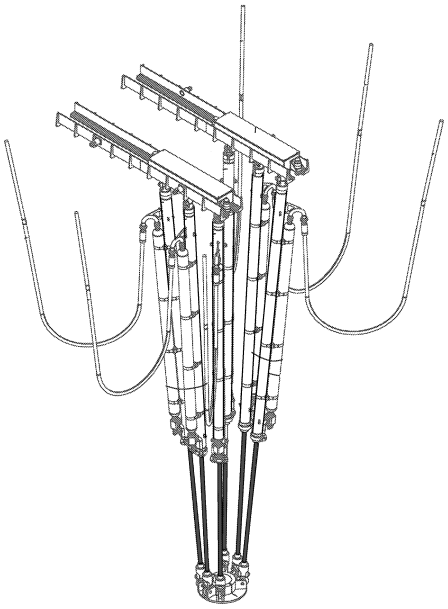

Fig. 2.3. Direct Acting Tensioner System [22]

2.1.2 Flex Joints

To reduce the bending moment on the riser and to allow angular misalignment between the riser and the BOP stack and motion of the rig, flex joints are installed both at the seabed and at the top of the slip joint. Flex joints consists of bonded laminations of elastomer which are placed between stacks of spherically shaped steel rings, to provide flexure and pressure sealing. It is known to be effective in terms of controlling riser angles, due to its rotational stiffness. To prevent damage to the riser, API and ISO have issued recommended practices for maximum flex joint angles during different phases, this is further explained in Chapter 2.3 [2].

2.1.3 Buoyancy Modules

Buoyancy modules are fitted along the length of the riser to reduce top tension requirements by reducing the submerged weight of riser joints. These modules are normally manufactured from low density composite synthetic foams with high compressive strength. The foam varies in density, to address the specific requirements of the riser buoyancy system, where the lightest are the premium type. These are designed to

reduce tensioner capacity requirements, reduce cross sectional areas of buoyancy and improve lift per riser joint. The buoyancy modules also has its downsides; the large diameter modules can cause stacking and storing challenges, as well as increased drag from currents [13].

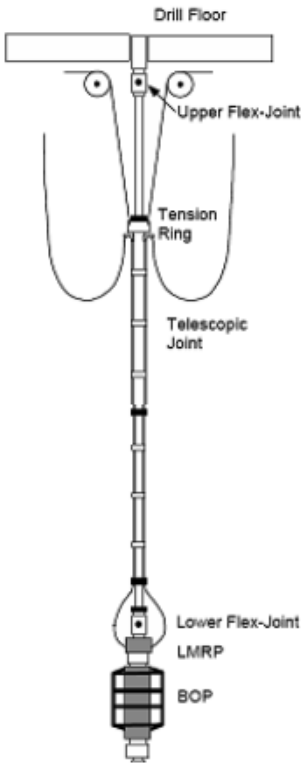

Fig. 2.4. A Typical Drilling Riser system with upper and lower flex joints [9]

2.1.4 Lower Marine Riser Package (LMRP)

The Lower Marine Riser Package typically comprises riser adapter, lower flex joint, annular rams, control pods that provides control of the BOP stack functions, hydraulic LMRP connector that attach the riser system to the BOP stack, and jumper hoses providing a flow path around the flex joint for the choke and kill lines. In addition the LMRP offers an Emergency Disconnect Package (EDP). The EDP serve as a disconnection point between the riser and the BOP stack. In case of an emergency and when required to do so the EDP needs to be able to disconnect quick, such as when unexpected extreme weather or other situations that can lead to rig drift-off occur [2].

2.2 Application of Alternative Materials

Today, steel is the conventional riser material. Steel is a heavy and very strong material with high tensile strength. However, as drilling activities extend into deep- (>600 m) and ultra-deep (>1500 m) waters with high-pressure and –temperature wells (HPHT wells) and sour reservoirs, a concern about the weight of thousands of meters of heavy steel pipe in the water and stored on deck arises. There is also a need to improve the corrosion resistance of the riser, as a result of more extreme reservoirs. Hence, the industry has its focus on how to reduce the weight of the riser without it being at the expense of safety and corrosion resistance [8, 2].

The focus has turned to the application of alternative materials. Aluminum, titanium and composite materials have been applied for riser design [12]. In this thesis the focus is on the aluminum and titanium, which are both well-known engineering materials. Some of the main characteristics and properties to the lighter materials are presented in the sections below.

2.2.1 Aluminum Riser

Aluminum is one of the most widely used light-weight construction materials, it is well known in aerospace, automotive, marine, and civil construction industries. In the oil & gas industry aluminum alloys have been used to develop drill pipe, tubing, casings and pipelines. In comparison with steel, aluminum alloys allows reducing structure weight and provide high overall corrosion resistance in different environments. Other known properties suitable for manufacturing marine drilling risers are [12]:

- High strength-to-weight ratio
- No brittleness at low temperatures
- No hydrogen embrittlement (resistance in environments containing hydrogen sulfide and carbon dioxide)
- Very good processing capabilities, in terms of machining, bending, pressing, extrusion, and fusion welding
- No cold-shortness at low temperatures (the problem of steel structures in arctic conditions)

2.2.2 Titanium Riser

Titanium has already successfully been used to fabricate drilling riser, flanges and booster lines for the Heidrun TLP in the Norwegian Sea. It proved to reduce both costs and weights for the project. Below are some of the observations that were made listed [17]:

- High strength-to-weight ratio
- High corrosion resistance
- Excellent fatigue properties (significantly higher endurance limit than steel)
- Low elastic modulus, resulting in lower stiffness than steel
- Similar machining characteristics to duplex steel
- Competitive lifetime costs because of reduced maintenance and reduction of loads on associated equipment
- Ten times higher wear rates for titanium against steel
- High manufacture costs

2.3 Standards and Regulations

The International Organization of Standardization (ISO) defines a standard as a document that provides requirements, specifications, guidelines or characteristics that can be used consistently to ensure that materials, products, processes and services are fit for their purpose.

In this section the API RP 16Q [2] and ISO 13624 [11] are presented. These standards includes a recommended practice for design, operation and maintenance of marine drilling riser systems.

2.3.1 API RP 16Q

The American Petroleum Institute (API) issued the first edition of the API RP 16Q in 1993, with the title «Recommended Practice for Design, Selection, Operation and Maintenance of Marine Drilling Riser Systems».

"This recommended practice pertains to the design, selection, operation, and maintenance of marine riser systems for floating drilling operations. Its purpose is to

serve as a reference for designers, for those who select system components, and for those who use and maintain the equipment. It relies on basic engineering principles and the accumulated experience of offshore operators, contractors, and manufacturer" [2].

Throughout the drilling operation the marine riser normally encounter the three following operating modes [2]:

- Drilling Mode - Is the combination of environmental and well conditions in which all normal drilling activities can be safely conducted.
- Connected Non-drilling Mode - In this mode, the drill pipe should not be rotated, and the only drilling operations which should be performed are circulating and tripping out drill pipe.
- Disconnected Mode - Occasionally the environmental conditions exceed the limits for safe operation in the connected non-drilling mode. In such conditions the the riser should be disconnected to avoid possible damage to surface or subsea equipment.

In Table 2.1 the recommended operating and design guidelines for the three operating modes are defined. It contains two stress criteria methods for the drilling mode, namely Method A and Method B, at least one of them should be satisfied. In general the former is appropriate for most water depth locations, and the latter is recommended for deep water locations. The table shows the allowable stress, where the stress criterion is the static stress plus maximum dynamic stress amplitude, and σ_y is the minimum yield strength of the material. The Stress Amplification Factor (SAF) is used to take the increase in the stresses in riser components caused by geometric stress amplifiers into account. All the stresses are calculated according to the von Mises stress failure criterion presented in Chapter 3.1.3.

The maximum flex joint angle limits for the connected non-drilling mode and disconnected mode are intended to prevent damage to the riser, flex joint and BOP stack. The upper flex joint angle rarely has a siginificant effect on riser design, however, this angle should be considered when evaluating clearance in the moonpool area.

In Chapter 2.1.1 the riser tensioners are discussed, these tensioners are required to ensure the stability of the riser. The API RP 16Q [2] recommend that the tension setting is kept sufficiently high so that the effective tension is always positive, in all parts of the riser, even if a tensioner should fail.

The minimum top tension, T_{min}, is determined by:

Table 2.1. Max. Operating and Design Guidelines from API RP 16Q [2]

Design Parameter	**Drilling Mode**	**Con. Non-drilling Mode**	**Disc. Mode**
Mean up. Flex jt. Angle	2.0 deg	N/A	N/A
Max. up. Flex jt. Angle	4.0 deg	90% avail.	på% avail.
Mean low. Flex jt. Angle	2.0 deg	N/A	N/A
Max. low. Flex jt. Angle	4.0 deg	90% avail.	90% avail.
Method A	0.4 σ_y	0.67 σ_y	0.67 σ_y
Method B	0.67 σ_y	0.67 σ_y	0.67 σ_y
SAF $\leq$ 1.5	69 MPa	N/A	N/A
SAF $>$ 1.5	15/SAF	N/A	N/A
Min. Top tension	T_{min}	T_{min}	N/A
Dynamic tension limit	DTL	DTL	N/A
Max. Tension setting	90% DTL	90% DTL	N/A

$$T_{min} = \frac{T_{SRmin}N}{R_f(N-n)} \tag{2.1}$$

and the Minimum Slip Ring Tension, T_{SRmin}, is determined by:

$$T_{SRmin} = W_s f_{wt} - B_n f_{bt} + A_i[d_m H_m - d_w H_w] \tag{2.2}$$

where W_s is the submerged riser weight above the point of consideration, f_{wt} is the submerged weight tolerance factor (min. value = 1.05, unless accurately weighed), B_n is the net lift of buoyancy material above the point of consideration, f_{bt} is the buoyancy loss and tolerance factor resulting from elastic compression, long term water absorption, and manufacturing tolerance (max. value = 0.96, unless accurately known), A_i is the internal cross sectional area of riser (including choke, kill, and auxilary fluid lines), d_m is the density of the drilling fluid, H_m is the drilling fluid column to the point of consideration, d_w is density of the sea water, H_w is the sea water column to the point of consideration (including storm surge and tide), N is the number of tensioners supporting the riser, n is the number of tensioners subject to sudden failure, and R_f is the reduction factor relating vertical tension at the slip ring to tensioner setting to account for fleet angle and mechanical efficiency (usually 0.9-0.95).

2.3.2 ISO 13624

Since the first edition of API RP 16Q was issued in 1993, the technology in this field has advanced, the equipment and methods has evolved and drilling in deep-water environments has increased significantly. Hence, it was necessary to update the code of practice to sufficient address the issues of deep-water drilling risers to supplement the API RP 16Q for drilling in water depths up to 3048 m. In that context the ISO 13624 was developed under the title «Petroleum and natural gas industries - Drilling and production equipment» in 2009, it consists of two parts, where part 1 examines the design and operation of marine drilling riser equipment, and part two examines deepwater drilling riser methodologies, operations, and integrity [11].

Table 2.2. Max. Operating and Design Guidelines from ISO 13624-1:2009 [11]

Design Parameter	**Drilling Mode**	**Con. Non-drilling Mode**	**Disc. Mode**
Mean up. Flex jt. Angle	1.0 to 1.5 deg	N/A	N/A
Max. up. Flex jt. Angle	5.0 deg	90% avail.	på% avail.
Mean low. Flex jt. Angle	2.0 deg	N/A	N/A
Max. low. Flex jt. Angle	5.0 deg	90% avail.	90% avail.
Method A	0.4 σ_y	0.67 σ_y	0.67 σ_y
Method B	0.67 σ_y	0.67 σ_y	0.67 σ_y
SAF $\leq$ 1.5	69 MPa	N/A	N/A
SAF $>$ 1.5	15/SAF	N/A	N/A
Min. Top tension	T_{min}	T_{min}	N/A
Dynamic tension limit	DTL	DTL	N/A
Max. Tension setting	90% DTL	90% DTL	N/A

When comparing the data in Table 2.2, which is the maximum operating and design guidelines from ISO 13624, with the data from API RP 16Q in Table 2.1, the limitations for upper and lower flex joint proves to be the most evident difference between the two. The mean upper flex jt. angle has been adjusted down to 1.0-1.5 deg. from 2.0 deg. and the maximum upper and lower flex jt. angle has increased from 4.0 to 5.0 deg.

It is necessary to keep the flex joint angles as small as practicable to avoid wear in the riser system components. According to the ISO standard the value 2.0 deg. in Table 2.2 is specified to include routine situations with low risk of significant wear, which could not continue with a more restrictive angle, and it is not uncommon that the mean differential angles are kept below 1 deg. [11].

Chapter 3

Fundamentals of Riser Mechanics and Hydrodynamic Loads

It is important to understand the influence of tension, pressure, and weight on the riser to get an adequate design. In addition the risers are exposed to harsh environment, making them prone to loads of considerable sizes, caused by sea currents, wave loads and drilling vessel movement. This chapter aims to explain the way marine drilling risers behave in such circumstances. The fundamental riser mechanics are explained and followed by the loads it experience due to hydrodynamic actions.

3.1 Riser Mechanics

As the riser extends from seabed to surface it experience several types of loading, the following sections focuses on the fundamental mechanics associated with the marine drilling riser. Starting with the much debated effective tension.

3.1.1 Effective Tension

One of the key concepts in marine riser engineering is the effective tension. Below is Archimedes' Law by superposition presented and followed by C.P Sparks' [19] simple relation between the true and effective tension, with the influence of internal and external pressures.

Archimedes' Law by Superposition

The Archimedes' principle states that when a body is wholly or partially submerged in a fluid, it experiences an upthrust, at the centroid of the displaced fluid (centroid

of the submerged body), equal to the weight of fluid displaced. It is important to be aware of that Archimedes' principle can only be applied directly to pressure fields that are completely closed, it cannot be applied to parts of a submerged body, and the law do not say anything about internal forces nor stresses [19].

If a body is immersed in a fluid by a string, the tension T in the string will be given bye the following, where W_t is the true weight of the body, W_f is the weight of the displaced fluid and $W_t - W_f$ is the apparent weight W_a :

$$T = W_t - W_f \tag{3.1}$$

Superposition is a more clearly and directly method to derive Archimedes' law. Fig. 3.1 shows the submerged body and the displaced fluid as two separate figures, which both are in equilibrium under the combined loads. The identical pressure fields can be eliminated by superposition of the two systems, as long as the displaced fluid segment represents the fluid displaced by the submerged body.

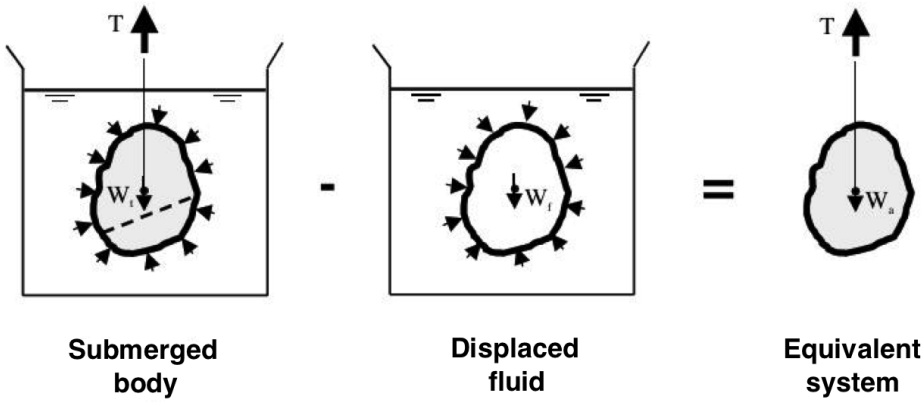

Fig. 3.1. Archimedes' law by superposition [19]

Internal Forces in a Submerged Body

Fig. 3.2 shows the internal forces acting on a submerged body segment and the forces acting on the displaced fluid segment. Archimedes' law cannot directly determine the internal forces on a segment of a submerged body, due to problems with taking the pressure field that is not closed into account. However, using superposition and subtract the forces on the displaced fluid from the forces on the body segment, the pressure field acting below the body is removed. The force from the pressure in the fluid p_e and the cross-sectional area of the section A_e, remains. Since tension and

compression is considered to be positive and negative, respectively, the force owing to the pressure acting on the section must be shown as a tensile force $-p_e A_e$. The right sketch in Fig. 3.2 is the result from the subtraction [19].

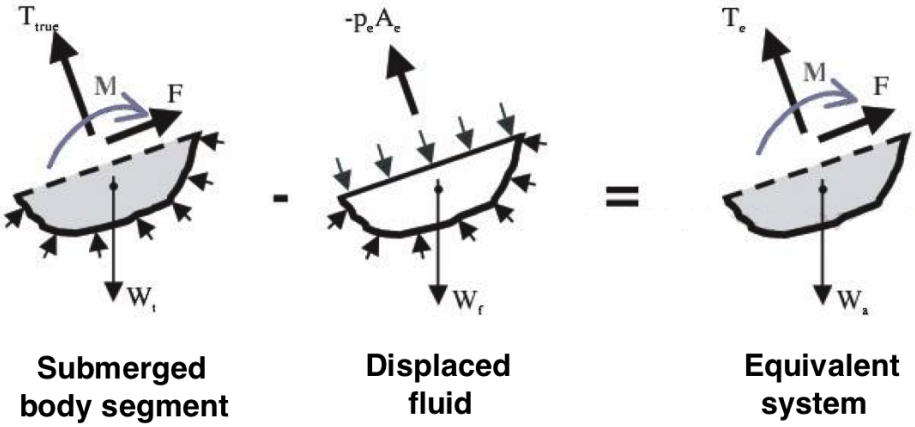

Fig. 3.2. Internal forces acting on a submerged body segment [19]

Since the weights W_t, W_f, and W_a now no longer represent the body, but the segment, the apparent weight is in equilibrium with an effective tension T_e, a moment M, and a shear force F. The effective tension T_e is the difference between the tensions acting on the body segment and the displaced fluid segment and can be given by the following [19]:

$$T_e = T_{true} - (-p_e A_e) = T_{true} + p_e A_e \tag{3.2}$$

Curvature, Deflections, and Stability of Risers under Pressure

The equivalent force system illustrated in Fig. 3.3 shows a riser represented by a curved pipe segment, with length δs, that is exposed to both internal and external pressure p_i and p_e, respectively, and a true wall tension T_{tw} acting in the pipe wall. The moments and shear forces have been neglected for simplicity. The closed pressure field acting on the internal fluid is in equilibrium with weight of the internal fluid, and the same but opposite to those acting on the internal wall. By adding the internal forces to the pipe segment and subtracting the forces from the external fluid, which is the displaced fluid, all lateral pressure effects are eliminated. C.P Sparks [19] derives the following equation for effective tension T_e and the apparent weight w_a:

$$T_e = T_{tw} + (-p_i A_i) - (-p_e A_e) = T_{tw} - p_i A_i + p_e A_e \tag{3.3}$$

$$w_a = w_t + w_i - w_e \tag{3.4}$$

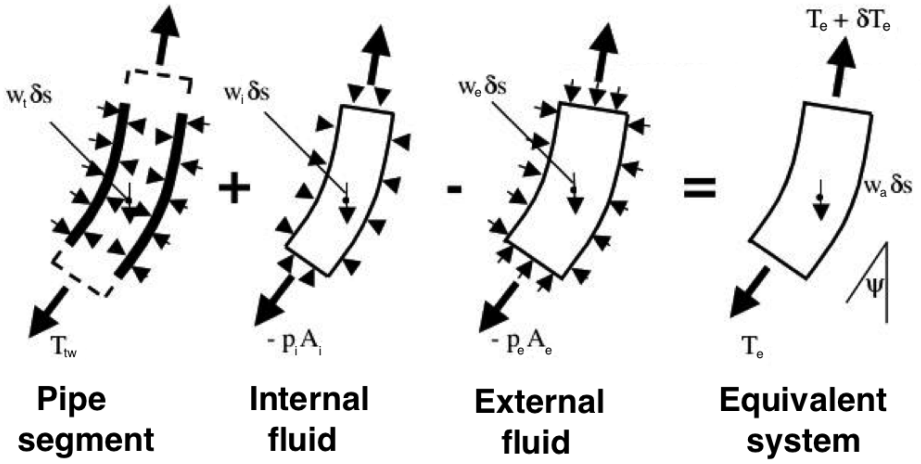

Fig. 3.3. Pipe with internal and external fluids and the equivalent force system [19]

Considering the same element with length δs and the angle Ψ with the vertical, the resolution of forces in the axial direction gives:

$$\frac{dT_e}{ds} = w_a cos\Psi \tag{3.5}$$

For small angles Eq. 3.5 becomes:

$$\frac{dT_e}{ds} = w_a \tag{3.6}$$

To obtain the effective tension at any point along the riser in a simple manner, the riser top tension and the apparent weight of the segment must be taken into account, as well as consider the equilibrium of the segment between the chosen point and the riser top end. Further, the true wall tension T_{tw} can be found from Eq. 3.3.

When a numerous of pipes are connected together, with some pipes within others, it gets more complicated, leading to the following equations for effective tension and apparent weight:

$$T_e = \sum T_{tw} + \sum(-p_i A_i) - \sum(-p_e A_e) \tag{3.7}$$

$$w_a = \sum w_t + \sum w_i - \sum w_e \tag{3.8}$$

From this C.P Sparks [19] deduce the following interpretation:
"Effective tension is the total axial force in the pipe/riser column, including internal fluid columns, less the axial force in the displaced fluid column (tension positive)"

3.1.2 Principal Stresses

The riser is considered to be a thick walled cylinder having an inner radius a and a wall thickness t. The cylinder is subjected to an axial load F_a, and pressurized with internal and external pressure p_a and p_b, respectively.

Tensile and compressive axial stresses are produced by axial loads and bending of the pipe. The pressure difference between inside and outside pressure gives rise to radial and hoop stress. The hoop stress σ_θ is the circumferential stress, axial stress σ_a is a the normal stress parallel to the axis of cylindrical symmetry, and the radial stress σ_r is coplanar but perpendicular to the symmetry axis. The thick walled cylinder and the stresses the wall experience is illustrated in Fig. 3.4.

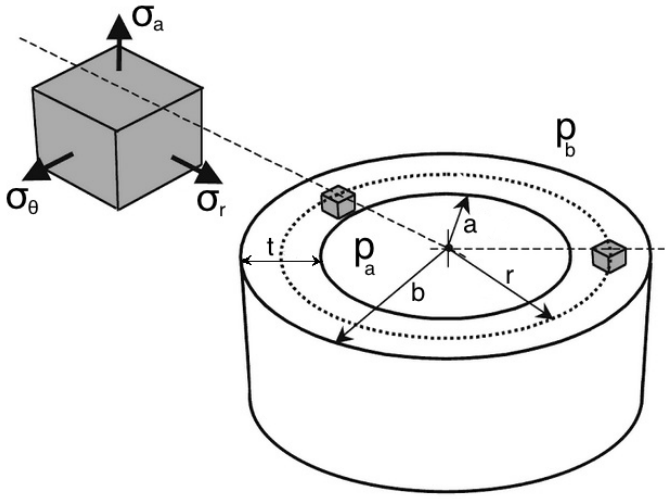

Fig. 3.4. In-wall Stresses [19]

To determine the stress distribution through the wall thickness, the stresses can be calculated using the equations developed by the French mathematician Gabriel Lamé. Lamé combined the following four conditions, equilibrium equation (Newton

law), compatibility relations (Strain and geometry relation), constitutive stress-strain-temperature relation (Hooke's law), and appropriate boundary condition. The resulting general equations known as Lamé's Equations are shown as follows [5]:

Hoop

$$\sigma_\theta = \frac{p_a a^2 - p_b b^2}{b^2 - a^2} + \frac{a^2 b^2}{(b^2 - a^2) r^2}(p_a - p_b) \tag{3.9}$$

Radial

$$\sigma_r = \frac{p_a a^2 - p_b b^2}{b^2 - a^2} - \frac{a^2 b^2}{(b^2 - a^2) r^2}(p_a - p_b) \tag{3.10}$$

Axial

$$\sigma_a = \frac{p_a a^2 - p_b b^2}{b^2 - a^2} + \frac{F_a}{\pi(b^2 - a^2)} \tag{3.11}$$

As mentioned the riser tensioners apply a continuous axial force to the riser to keep it in tension and avoid buckling and collapse. This axial force (F_a) contributes to the axial stress. Fig. 3.5 illustrates the stress distribution across the wall thickness (Eq. 3.9-3.1.2).

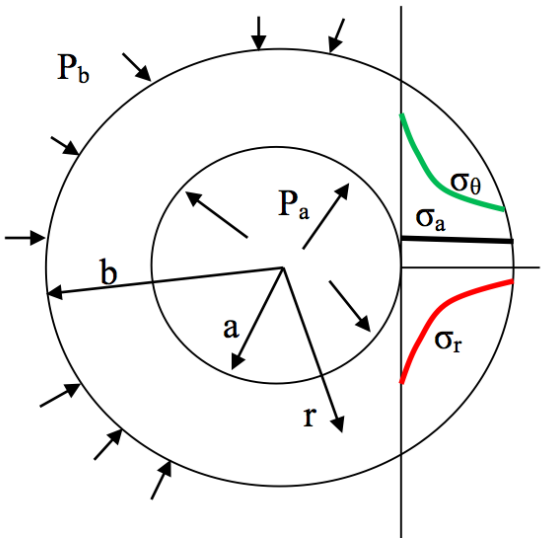

Fig. 3.5. The stress distribution in a thick-walled cylinder when $P_a > P_b$ [5]

Shear Stress

The shear stress τ is the component of stress coplanar with the pipes cross section. Shear stresses in the riser may be caused by torque which can arise from floating drilling rig movement. Shear stress is force (torque, T) per unit area.

$$\tau = \frac{T}{2\pi a^2 t} \tag{3.12}$$

Bending Stress

Marine riser are exposed to bending moments arising from drilling rig motions caused by waves, winds, and currents. The bending stress is the primary contributor to riser fatigue. Riser bending is primarily occurring in the lower most riser joint, connected to the lower flex joint, and the maximum bending stress occurs at the outer diameter of the pipe. In order to derive the expression for the bending stress the beam theory is used [3].

$$\sigma_b = \frac{M}{I} y \tag{3.13}$$

Where σ_b is the bending stress, M is the bending moment, I is the moment of inertia, and y is the distance to the center of the pipe.

3.1.3 Von Mises Failure Criterion

The von Mises Failure Criterion is considered to be the most accurate criterion for the combination of stresses that provokes the beginning of yield in ductile materials. All the stresses in the API and ISO standards presented in Chapter 2.3 are calculated according and refer to the von Mises stress criterion, this also applies to the simulation software used in Chapter 4.

The criterion is based on the determination of the distortion energy in a given material. The riser manufacturer performs tensile tests specified on the same material as being used in the riser to find the distortion energy per unit volume required to cause yield σ_y, according to the von Mises criterion the material is safe as long as the maximum value of the distortion energy per unit volume σ_{von} remains smaller than the results from the tensile test.

In general the onset of yield for a riser is based on the combination of the three in wall stresses (σ_θ, σ_r, and σ_a) presented in Fig. 3.4 and the potential shear stress τ caused by torque , it can be expressed [5]:

$$\sigma_{von} = \sqrt{\frac{1}{2}\left\{(\sigma_\theta - \sigma_r)^2 + (\sigma_r - \sigma_a)^2 + (\sigma_a - \sigma_\theta)^2\right\} + 3\tau^3} \tag{3.14}$$

When taking the bending moments the riser experience into account the bending stress σ_b is added to the axial stress σ_a, and Eq. 3.14 becomes:

$$\sigma_{von} = \sqrt{\frac{1}{2}\left\{(\sigma_\theta - \sigma_r)^2 + (\sigma_r - (\sigma_a + \sigma_b))^2 + ((\sigma_a + \sigma_b) - \sigma_\theta)^2\right\} + 3\tau^3} \tag{3.15}$$

When the σ_{von} exceeds the yield stress σ_y of the material the yielding starts to occur.

3.2 Hydrodynamic Loads

The riser system must withstand the impact from interaction between strong currents and waves. To determine these loads and the following impact from the environment, it is important to understand the environmental conditions and how the environmental loads behave.

3.2.1 Waves

Waves in the ocean varies and are irregular in height, length, shape, and speed of propagation. Hence, the best description of the sea state is by a random wave model. In a wave condition the sea state can be divided into two groups, wind seas and swell. Wind seas are a result of local wind blowing over an area. The swell on the other hand have no relation to local wind, they are generated in other areas and travels out from their origin. In addition, swell state can be generated by several swell components from different areas [7].

A regular traveling wave is propagating with a permanent form, and it has a distinct wave length, wave period, and wave height. The wave length λ is the distance between successive crest, wave period T is the time interval between successive crest passing a

particular point, and the wave height H is the vertical distance from trough to crest, and can be found by:

$$H = A_C + A_T \tag{3.16}$$

Where A_C is the distance from the still water level to the crest also known as crest hight, and A_T is the through depth, which is the distance from the still water level to the through. Other important wave characteristics are listed below:

Phase velocity, c: Is the propagation velocity of the wave form, also known as wave speed and wave celerity. It is equal to λ/T.
Wave frequency, f: Is the inverse of wave period, $1/T$.
Wave angular frequency, ω: Is equal to $2\pi/T$.
Wave number, k: Is equal to $2\pi/\lambda$.
Surface elevation, z: Is the distance between the still water level and the wave surface, $z = \eta(x, y, t)$.

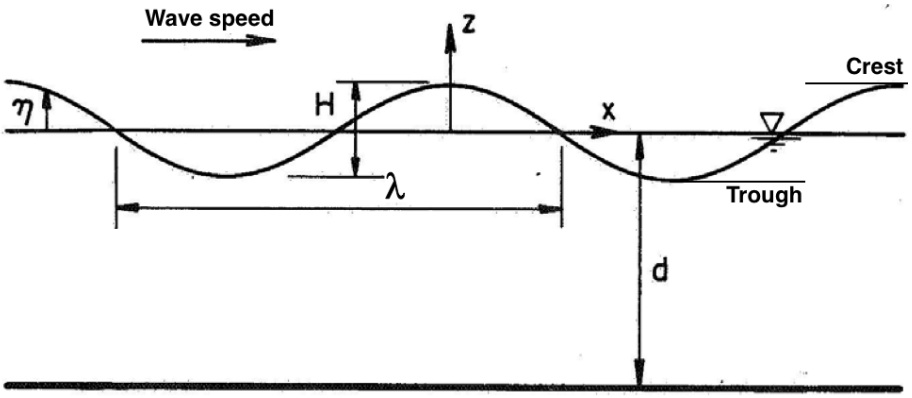

Fig. 3.6. Regular traveling wave characteristics [7]

3.2.2 Currents

For deep water marine drilling the riser is particularly influenced by currents. The currents can give rise to drag and lift forces on the submerged riser, and to vortex induced vibrations (discussed in the following section, 3.2.3). The external forces the currents induce can change the deflection of the riser, thus influencing the tension

and drilling vessel position. Hence, effects of currents are important to consider and understand for an adequate riser design.

Currents can be divided in to several categories, some of the most common are wind generated currents caused by wind stress and atmospheric pressure gradient throughout a storm, tidal currents that are regular currents following the harmonic astronomical motions of the planets, circulational currents, which are steady and large scale currents of the general oceanic circulation, and loop and eddy currents formed by separated parts of circulation currents [7].

The current velocity vector varies with water depth, and due to surface waves, the current velocity profile is stretched or compressed close to the water surface. The site specific measurements should extend over the water column and over the period that captures several major storms. Despite the importance of information on statistical distribution of currents and their velocity profile, there is lack of this data in certain areas. The current profile should be varied during the analysis to determine the sensitivity of the results to current profile shape. If sufficient data is not available conservative values, using combined events should be applied [7].

3.2.3 Vortex Induced Vibrations (VIV)

Flow passing slender objects, such as a marine drilling risers, may cause unsteady flow patterns due to vortex shedding. In harsh environments this dynamic condition can be a source of problems during extended operations. During operations in deep waters the riser is particularly prone to VIV and the riser is much more dependent upon the shape of the current profile width depth, because currents are typically higher in deepwater areas than in shallower areas, in addition the increased length of the riser lowers it natural frequency derby lowering the magnitude of current required to excite VIV. Vortex Induced Vibrations may cause resonant axial vibrations in deep sea risers. Such axial vibrations can lead to excessive stresses in the riser and may cause the riser system to experience significant fatigue damage [1].

3.2.4 Morison Equation

The Morison Equation can be used to calculate the combined effects of current and wave loads on small-diameter submerged objects such as the marine riser. The results are considered to be reasonable accurate in situations where the riser diameter is small compared to the wavelength (ratio between the wave length and tubular diameter is greater than 5 [20]). The hydrodynamic force f_H in Eq. 3.17 is the sum of two force

components, a drag force f_D and an inertia force f_i, resulting from the velocity of the flow past the body, and from the acceleration of the flow, respectively [19]:

$$f_H = f_D + f_I \tag{3.17}$$

From laboratory investigation it has been found that for steady flow the drag force f_D varies with the square of the velocity. For risers, exposed to flow normal to its axis, f_D per unit length is given by:

$$f_D = \frac{1}{2}\rho C_D \phi u|u| \tag{3.18}$$

Where ρ is the fluid density, C_D is the non-dimensional drag coefficient that varies with the body shape and Reynolds number (typical value for laminar flow is 1.0, and about 0.6-0.7 for turbulent flow), ϕ is the diameter of the body, and u is the instantaneous velocity of the fluid normal to the cylinder axis.

For a riser that is itself moving laterally with the velocity v in the direction of the flow, the relative velocity must be used in Eq. 3.18, which then becomes:

$$f_D = \frac{1}{2}\rho C_D \phi (u - v)|u - v| \tag{3.19}$$

For a volume V of fluid width a density ρ experiencing a uniform acceleration $\dot{u}$, the dynamic pressure field acting on it must apply an inertia force f_I given by:

$$f_I = \rho V \dot{u} \tag{3.20}$$

Through extensively laboratory tests a non-dimensional inertia coefficient C_M has been found, and for a smooth cylinder, at high Reynolds number C_M is typically close to 2.0. For a stationary sphere of volume V subjected to accelerating flow Eq. 3.20 then becomes:

$$f_I = C_M \rho V \dot{u} \tag{3.21}$$

By decomposing the inertia force into into two parts, the hydrodynamic force acting on the displaced fluid in the absence of the sphere ($\rho V\dot{u}$), and an additional force $(C_M - 1)\rho V\dot{u}$ caused by the acceleration of the fluid relative to the sphere. And if the spehere itself is moving with acceleration $\dot{v}$ in the same direction as the fluid the relative acceleration becomes $\dot{u} - \dot{v}$ and Eq. 3.21 becomes:

$$f_I = \rho V\dot{u} + (C_M - 1)\rho V(\dot{u} - \dot{v}) \tag{3.22}$$

If V is replaced by the external cross-sectional area A_e, Eq. 3.22 can be used to give the inertia force per unit length of a riser subject to wave action. Hence, by inserting Eq. 3.19 and 3.22 into the initial Morison equation (Eq. 3.17) it can be written as either of the following:

$$f_H = \frac{1}{2}\rho C_D\phi(u - v)|u - v| + \rho A_e\dot{u} + (C_M - 1)\rho A_e(\dot{u} - \dot{v}) \tag{3.23}$$

$$f_H = \frac{1}{2}\rho C_D\phi(u - v)|u - v| + C_M\rho A_e\dot{u} - (C_M - 1)\rho A_e\dot{v} \tag{3.24}$$

Marine drilling riser are in most cases equipped with kill and choke lines, making the geometries more complicated than bare pipe. Hence, an equivalent diameter ϕ and an equivalent cross-sectional area A_e must be applied in the Morison equation [19].

The simulation software OrcaFlex, used in Chapter 5, calculates hydrodynamic loads using an extended form of the Morison Equation. This extended form can be expressed [16]:

$$F_f = \frac{1}{2}\rho C_d A V_r|V_r| + (\Delta a_f + C_a\Delta a_r) \tag{3.25}$$

where F_f is the fluid force, Δ is the mass of fluid displaced by the body, a_f is the fluid acceleration relative to earth, C_a is the added mass coefficient for the body, a_r is the fluid acceleration relative to the body, ρ is the density of water, V_r is the fluid velocity relative to the body, C_d is the drag coefficient for the body, and A is the drag area. The term in the parentheses is the inertia force, and the other term is the drag force.

Chapter 4

Simulation Study

To imitate and give insight in how the marine drilling riser behave under certain conditions a simulation software models a real phenomena with a set of mathematical formulas. It allows the user to observe an operation through simulation, and that way aiding the user in design and analysis, while saving time and resources.

This simulation study emphasizes the harsh environment in the Norwegian Sea, more specifically the location of the deep water Aasta Hansteen gas field. First, the environmental data provided by Statoil is presented and described, before a brief description of the simulation software OrcaFlex takes place and the build-up of the model is described in more detail.

4.1 The Norwegian Sea: Aasta Hansteen field

The Norwegian Sea is one out of three regions on the Norwegian Continental Shelf (NCS), it is a marginal sea in the North Atlantic Ocean, and is located northwest of Norway. The area has since the first field came on stream in 1993 produced more than 585 million standard cubic meters of oil and 454 billion standard cubic meters of gas. The vast ocean area still contains large amounts of oil and gas to be discovered. The remaining resources are estimated to contain about 25 % of the remaining resources on the NCS. These undiscovered resources are probably located in the more unconventional areas of the Norwegian Sea. The environment in the 287 000 square kilometers the Norwegian Sea covers can be harsh, with waves exceeding 30 meter, wind speeds up to 39 m/s, and sea currents up to 1.8 m/s. These factors undoubtedly make the Norwegian Sea a quite demanding area for drilling operations and recovery of resources. The particularly harsh environment in the Norwegian Sea makes it an interesting location to perform simulation studies [15].

Aasta Hansteen is a gas field located in the deeper waters of the Norwegian Sea (67.07° N 07.01° E), the water depth is around 1200 m. The field was discovered in 1997, however, the plan for development and operations was not submitted before the end of 2012, and the drilling of the production wells are not planned to start before the beginning of 2018. The field is located far from land and outside established infrastructure, with significant water depths and challenging weather conditions the recovery of resources are demanding [15].

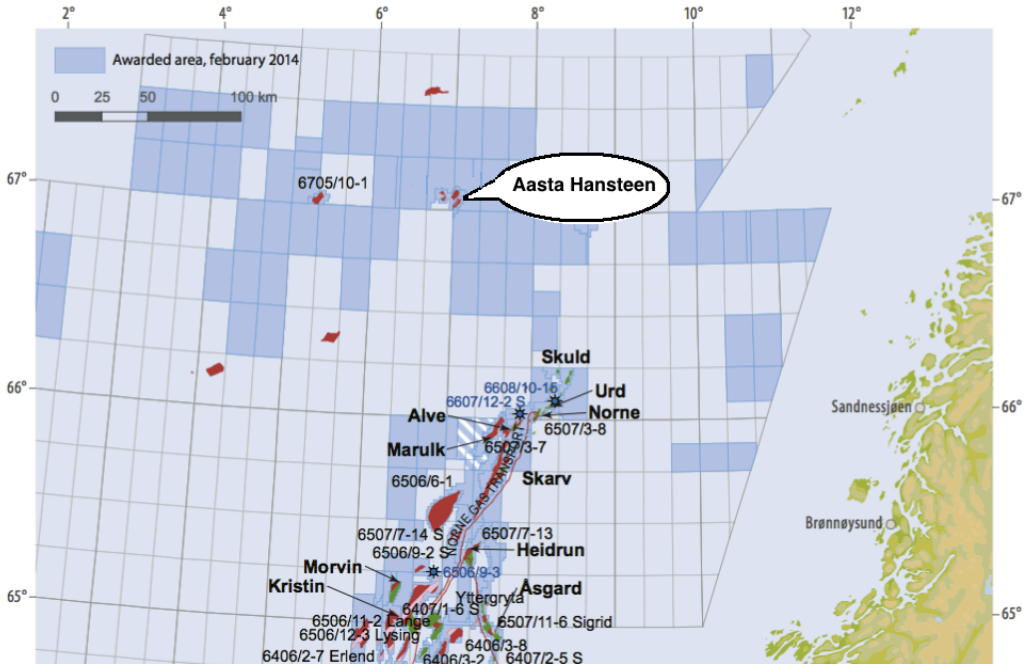

Fig. 4.1. Map showing the position of Aasta Hansteen Field in the Norwegian Sea [14]

Reliable historical weather data (wind, waves, and currents) are important during the design of riser systems and when planning drilling operations, to recreate past conditions as accurately as possible. A hindcast model operated by the Norwegian Meteorological Institute uses historical data as input values to see how well the output from the model matches the known results. The data chosen for analysis in this thesis are taken from the «Aasta Hansteen Metocean Design Basis», provided by Statoil. The wind and wave data are from the NORA10 hindcast model, at the grid point 67.05° N, 07.00° E. The period covered is 1958-2008, and the sample interval is 3 hours [21].

4.1.1 Wind

Drilling operations may be delayed or aborted due to wind speeds exceeding prescribed operational limits leading to a possible expensive stop or increased duration of the operation. Fig. 4.2 shows the percentage of wind observations within each 30° sector for the period 1958-2008 at the Aasta Hanseen Field area. The wind direction is given in degrees [°] and is the direction from which the wind is blowing, measured clockwise from north, (e.g. winds of direction 90° is coming from the east). The most powerful winds are in the winter months January, February, and December [21].

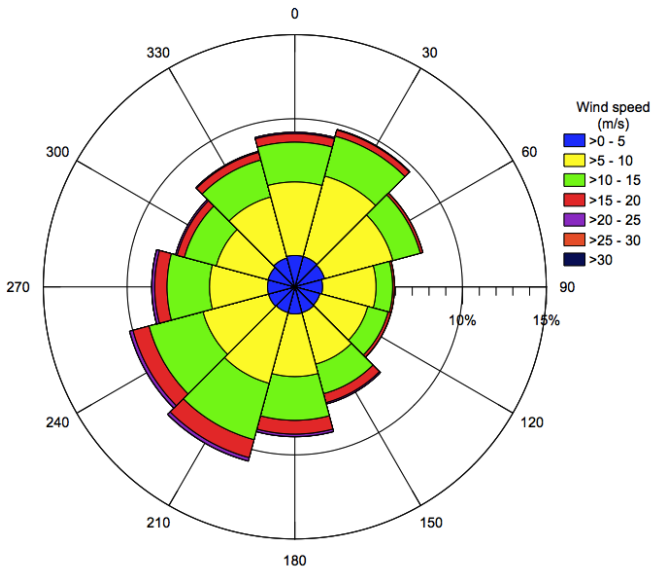

Fig. 4.2. All-year wind rose for the Aasta Hansteen Field for the period 1958-2008 [21]

The wind distribution is is widely spread in all direction periods, however the biggest contributer is the winds from southwest. in Table 4.1 the the annual probability for extreme wind speeds are presented.

Table 4.1. Annual probability for extreme wind speed [21]

Annual probabilty of exceedance	**Extreme wind speed values (m/s)**
0.63	28
10^{-1}	31
10^{-2}	34
10^{-4}	39

4.1.2 Waves

As for the wind, wave heights exceeding prescribed operational limits may delay or cause unwanted interruptions in the drilling operations. Fig. 4.3 shows the sample direction distribution of significant wave heights H_s within each 30° sector for the period 1958-2008 at the Aasta Hanseen Field area. Significant wave height H_s is the average height of the 1/3 highest measured waves. The wave direction is given in degrees [°] and is the direction from which the waves are coming, measured clockwise from north, (e.g. waves of direction 90° is coming from the east).

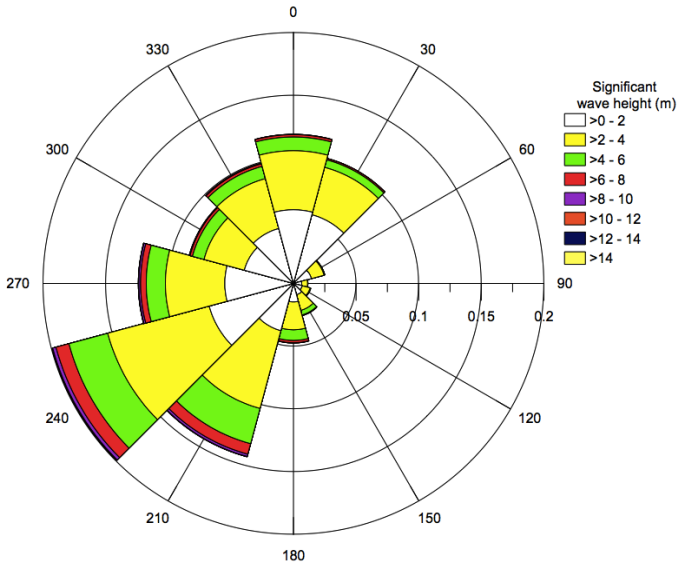

Fig. 4.3. All-year wave rose for the Aasta Hansteen Field for the period 1958-2008 [21]

From Fig. 4.3 one can read that most of the values are in the 240° period, meaning that the vast majority of the waves are coming from southwest. The roughest seas with the maximum significant waves heights are during the winter season, especially in January and February, where the maximum significant wave heights are up to 14.8 meters. Table 4.2 presents the spectral peak period T_p for a given set of significant wave heights H_s.

Table 4.3 presents the annual probability for extreme wave heights and the corresponding spectral peak periods. The statistically projected wave probability is often expressed as a return period. For structural design a 10-year or/and 100-year return period data are used. In other words the probability for 10- and 100-year waves are 0.1 and 0.001, respectively.

Table 4.2. Spectral peak period T_p as a function of significant wave height H_s at the Aasta Hansteen Field [21]

Significant wave height H_S – (m)	**Mean spectrall peak period T_p – (s)**
1	8.2
2	9.3
3	10.2
4	11
5	11.8
6	12.4
7	13.1
8	13.7
9	14.3
10	14.9
11	15.4
12	16
13	16.6
14	17.1
15	17.6
16	18.2
17	18.7

Table 4.3. Extreme significant wave heights and corresponding spectral peak periods [21]

Annual probabilty of exceedance	**Significant wave height H_S (m)**	**Spectral peak period T_p (s)**
0.63	11.8	15.9
10^{-1}	14.3	17.3
10^{-2}	16.7	18.5
10^{-4}	21.3	20.9

4.1.3 Currents

In the upper layer of the Norwegian Sea, warm, saline water from the North Atlantic flows northward, this current is referred to as the Norwegian Atlantic Current. The surface currents are characterized by the branches of this current. At greater depths cold bottom water formed in the Greenland Sea flows back to the Atlantic [4].

The current data in this thesis are from measurements at the Aasta Hansteen Field in different periods between 2008 and 2012 with 10 minute sample intervals. The maximum water depth in the area is 1290m. Data from these measurements are shown in Table 4.4 from 20 meter water depth down to 3 meter above sea bottom (asb). Gaps in the data series reduces the effective length of the measurement. Due to the relatively short duration of measurements there will be uncertainties associated with predicted extremes [21].

Table 4.4. Max. and mean currents speeds measured at the Aasta Hansteen field

Depth (m)	**Max current speed** (cm/s)	**Mean current spead** (cm/s)
20	101	21.6
50	99	20.81
100	93	19.09
200	86	18.14
300	67	16.76
400	80	16.66
500	59	14.47
600	46	13.01
800	52	13.22
1000	53	12.28
1200	48	12.05
3 m asb	45	10.64

In the upper part close to the surface the currents flows from all different directions, while at greater depths the currents tend to flow more west. The current direction is given in degrees [°] and is the direction towards which the current is flowing, measured clockwise from north, (e.g. currents of direction 90° are towards the east).

4.2 OrcaFlex

The dynamic simulations in this thesis are performed using OrcaFlex. The simulation program is used to build an offshore drilling rig model with a tensioned marine drilling riser extending from seabed to surface. The model is used to simulate the loads, forces, displacements and angles the riser experience with different materials, various top tension and drilling fluid densities at different loading scenarios. The surrounding environment and water depth is modelled to be similar to the deep-water Aasta Hansteen gas field.

OrcaFlex is developed by Orcina and is considered as one of the world's leading packages for dynamic analysis of offshore marine systems. It works by building a mathematical computer model of the desired system. The model is built up from a series of interconnected objects (e.g. vessel, riser, buoys, and lines). However, it is important to note that software programs are not intelligent, it is the user who is, and the input determines the output. Hence, the quality of the output is never better than the input.

4.2.1 Coordinate System

OrcaFlex uses a global coordinate system GXYZ (where G is the global origin and GX, GY and GZ are the global axes direction). In addition, every object in the model have a local coordinate system denoted by Lxyz, see Fig. 4.4. Also the seabed has its own origin and local axes, with respect to which the seabed shape is defined.

OrcaFlex allows objects to be connected to other objects, where one is designated as the master and the other is designated as the slave. The master object determines the position of its slave. As the master moves the slave is dragged around, in response the slave applies forces and moments to its master. In addition, objects can also be fixed (connected to the global axis) or anchored (connected to the seabed).

Directions and headings are specified by giving the azimuth angle of the direction, in degrees, measured positive from the x-axis towards the y-axis. The directions for wind, waves, and current are specified by giving the direction in which they are progressing, relative to global axes [16].

4.2.2 Marine Drilling Riser Structural Model

The drilling riser system constructed in OrcaFlex is for this thesis based on the drilling riser example provided by Orcina on orcina.com. The system consists of a drilling

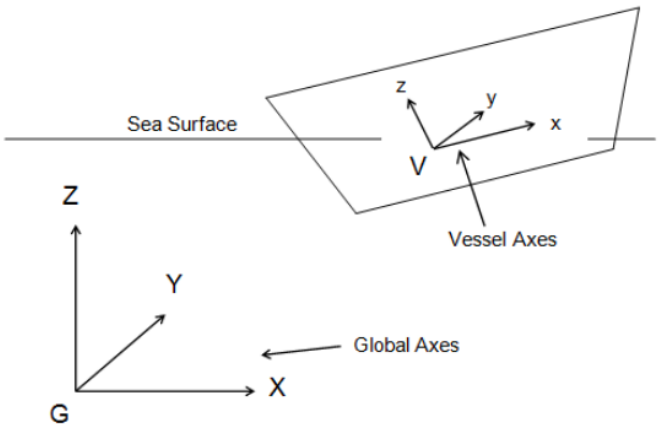

Fig. 4.4. OrcaFlex Coordinate System [16]

vessel, tensioner system, telescopic joint, upper flex joint, pup joints, riser joints, kill or/and choke lines, lower flex joint, LMRP, and BOP. A schematic overview of the drilling riser system is shown in Fig. 4.5, for simplification purposes it does not include kill or choke lines nor conductor pipe.

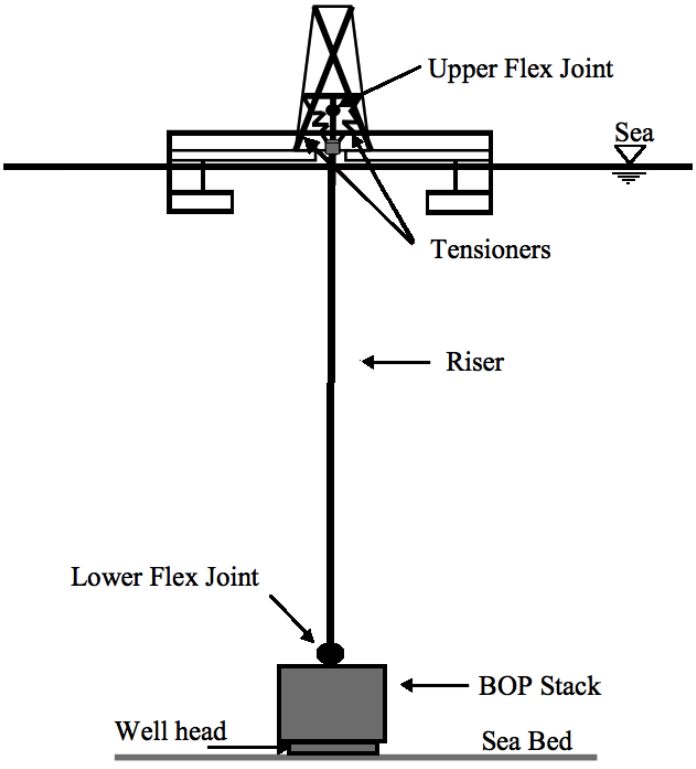

Fig. 4.5. Schematic Diagram of the Drilling Riser System

Vessel

The drilling vessel in OrcaFlex is modelled as a semi-submersible drilling rig. The moonpool edges are modelled as dummy lines to obtain the clearance information between the moonpool and tensioners, riser, choke or kill lines. The deck structures have zero stiffness and are there for visualization only. This model has not focused on the visual, and since the structures don't effect the result they have stayed unchanged from OrcaFlexs' default settings. Fig. 4.6 shows the vessel in OrcaFlex.

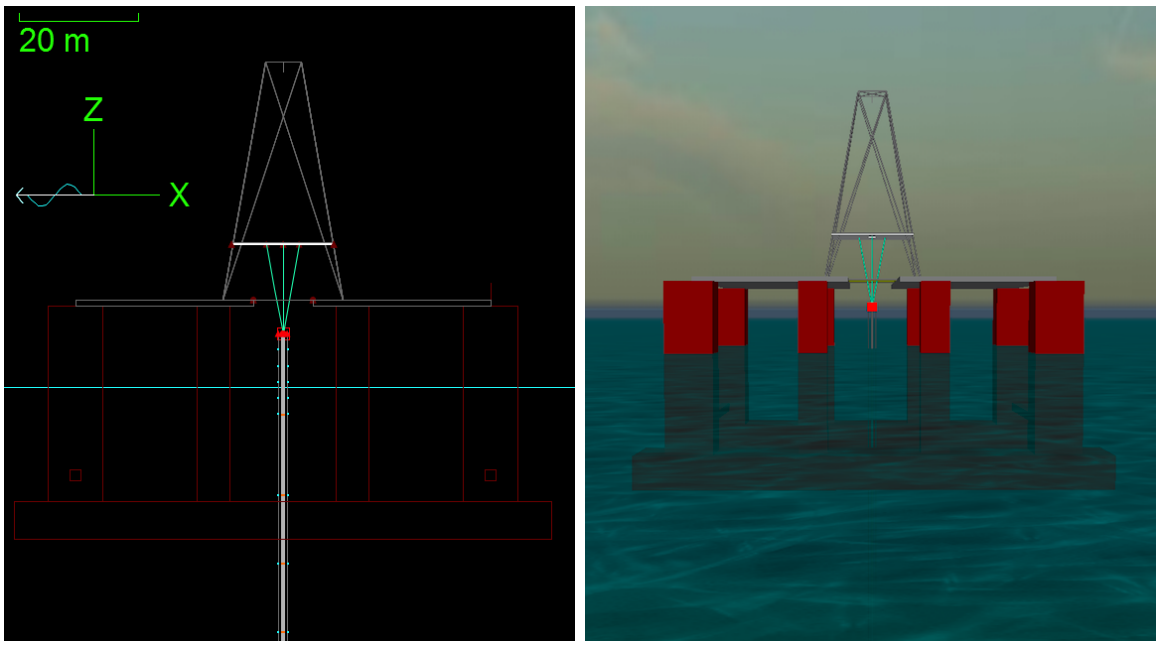

(a) 2D **(b)** 3D

Fig. 4.6. Drilling vessel in OrcaFlex

Tensioner system

The tensioner system is modelled by using 4 nonlinear spring elements. The elements are links with no mass or hydrodynamic loading, they link two points in the model and simply apply an equal and opposite force to the two points. The force characteristic is specified as a table of tension against length.

The tensioners are connected to the vessel in one end and to the tensioner ring in the other end. The tensioner ring is modelled as a 6D buoy, which has all six degrees of freedom, and both mass and moments of inertia. As the only purpose the tensioner ring has in this model is to serve as a connection point for tensioners, riser and kill and choke lines, the buoy is set to have negligible properties.

Riser joints

The marine drilling riser and the two auxiliary lines are modelled as line elements in OrcaFlex. The lines are divided into a series of line segments, these are then modelled by straight massless model segments with a node at each end. They are all connected to the tensioner ring at the top, and extend all the way down to the to the lower flex joint. The choke and kill lines each have a line contact relationship defined with the riser, which enables the lines to be clamped to each other at specified locations. The riser restraints goes around the choke and kill lines. The lower flex joint is modelled as a 6D buoy to ensure that the BOP sees appropriate total moments. The BOP is represented by a cylindrical object. Fig. 4.7 shows a finite element model Orcaflex uses for lines.

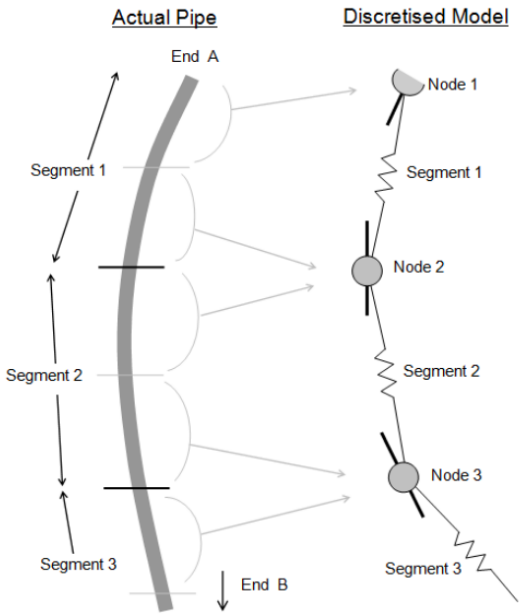

Fig. 4.7. OrcaFlex line model [16]

The structural configuration of the marine drilling riser is shown in Table 4.5, where OD is the outer diameter, and ID is the innder diameter.

Table 4.5. Structural Configuration of Drilling Riser

Type	No. of joints	Length (m)	Total length (m)	OD (m)	ID (m)
Pup joint	2	13.5	27	0.533	0.489
Riser joint	51	23	1173	0.533	0.489
Kill/chk. line	1	1200	1200	0.127	0.095

In this work the marine drilling riser simulations are carried out for a conventional steel riser and the less common riser materials aluminum and titanium. The peripheral kill and choke lines are modelled with the same material properties and internal fluid as the riser. The different material properties are shown in Table 4.6 [12, 23].

Table 4.6. Riser Material Properties

	Steel	**Aluminum**	**Titanium**
Density (kg/m^3)	7850	2700	4480
Young's Modulus (GPa)	207	69	107
Poissons ratio	0.293	0.334	0.32
Yield Strength (MPa)	560	350	483
API & ISO = 0,67σ_y (MPa)	375.2	234.5	323.61

4.2.3 Modelling of Environmental Loading

The environmental modelling plays a very important role in offshore design. Nature is unpredictable, causing major uncertainties when it comes to environmental loading, making the input data very important. This thesis emphases the simulation study to the deeper waters of the Norwegian Sea. The environmental data are gathered from the Aasta Hansteen field, in an area where the water depth is approximately 1200 m, the data is provided by Statoil. 1-year and/or 10-year return period data for environmental loading parameters are the current industry practice of deterministic design used for structural design for the drilling location [18].

Current

In the presence of waves, OrcaFlex extrapolate the current above still water level by the convention that the surface current applies to all levels above the still water level.

The Power Law Method is used to model the currents. In this method the current direction is specified and does not vary with depth, it is set to the same direction as the wind and waves, namely 180°. In other words, from bow to stern. The current speed S varies with position (X,Y,Z) according to the following equation, where S_f and S_b are the current speeds at the surface and seabed, respectively. k is the power law exponent, Z_f is the water surface Z level and Z_b is the Z level of the seabed directly below (X,Y) [16]:

$$S = S_b + (S_f - S_b) \times \Big((Z - Z_b)/(Z_f - Z_b) \Big)^{1/k} \tag{4.1}$$

As mentioned above the current direction is the same in all levels, and the direction is specified as the direction the current is progressing, measured positive from the global X-axis towards the global Y-axis. The exponent k determines how the current decays. With a smaller k value, the decay is spread more evenly across the water depth, and for a higher value the decay mostly occurs close to the seabed. A reasonable value for k is 0.3.

From Eq. 4.1 the current velocity distribution from surface to seabed is obtained. The input values for S_f and S_b are set to the highest observed surface and seabed velocities (101 cm/s and 45 cm/s, respectively), at the Aasta Hansteen Field, and exponent k is set to 0.3. The current velocity distribution is shown in Fig. 4.8.

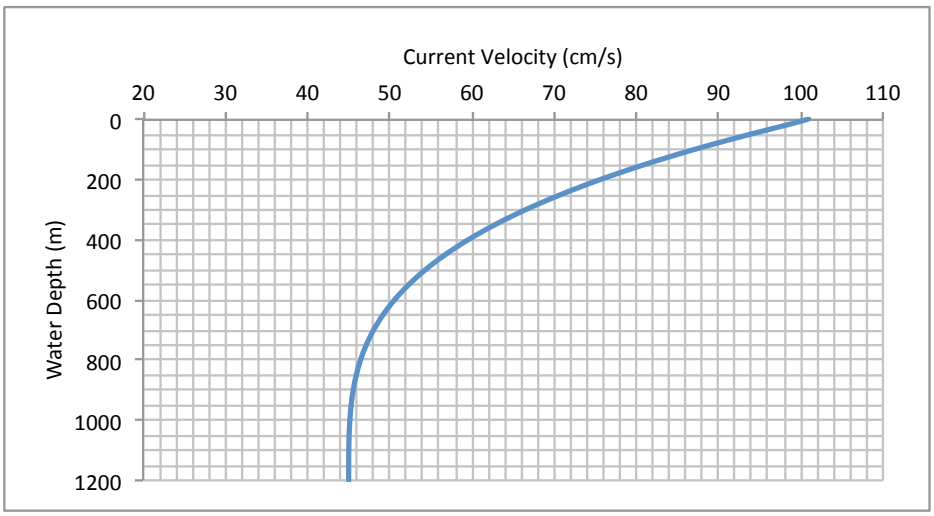

Fig. 4.8. Current Velocity Distribution

Wave

In OrcaFlex it is possible to define a number of different wave trains and the overall sea conditions are the superposition of the wave trains. In this case a single wave train is considered sufficient. The wave train can either be a regular wave (with a choice of wave theory), a random wave (with a choice of spectrum), specified by a time history file or specified explicitly by a list of components. The wave train is specified by wave direction, wave type, wave origin and wave time origin.

Wave direction is the direction that the wave is progressing, measured positive anti-clockwise from the global X-axis when viewed from above. This applies to both regular and random waves. It is set to 180°for all simulations.
Wave types are different for regular waves and random waves. The former can be Airy, Dean, Stokes' 5th or Cnoidal, and random waves can be JONSWAP, ISSC, Ochi-Hubble, Torsethaugen, Gaussian Swell or User Defined Spectrum. For regular waves OrcaFlex recommend the Dean wave, which is a non-linear wave theory using a Fourier approximation method and it is suitable for all regular waves. Although a random wave model is the most realistic description of the sea state, regular waves are more conservative when it comes to simulation output. Hence the waves are modelled as regular Dean waves.
Wave spatial origin and **wave time origin** is specified relative to the global origin and relative to the global time origin, respectively. For a regular wave train the wave time origin is the time at which a wave crest passes the wave origin.

A regular design wave is a single wave component and is defined by wave height H, period T, and direction. To produce a realistic wave train a method described in NORSOK N-003 and illustrated below can be used to calculated the period for each wave height [20].

$$\sqrt{6.5H} \leq T \leq \sqrt{11H} \tag{4.2}$$

Table 4.7 shows the wave input data obtained from Eq. 4.2. This data is used in some of the simulations. The seven meter wave in the table below is used in addition to the 1-year and 10-year return period waves presented in Chapter 4.1.2.

Table 4.7. Design Wave heights and periods

Wave Height, $H(m)$	1	2	3	4	5	6	7	8	9	10	11.8
Wave Period, $T(s)$	3	5	5	6	6	7	7	8	8	9	10

Wind Data

The wind speed is for all the simulations set to the highest value for 10-year return period at the given location, which is 31 m/s. The direction of the wind is 180°.

4.2.4 Static Analysis and Dynamic Analysis

To determine the equilibrium configuration of the system under weight, buoyancy, hydrodynamic drag, etc. and to provide a starting configuration for the dynamic simulation, a static analysis is performed. In a series of iterative stages the static equilibrium is determined. At the start of the calculation, the initial positions of the vessels and buoys are defined by the data, these in turn define the initial positions of the ends of any lines connected to them. The out of balance load acting on each free body (node, buoy, etc.) is then calculated and a new position for the body is estimated. The process is repeated until the out of balance load on each free body is zero (up to the specified tolerance) [16].

The dynamic analysis is offered in two different approaches: time domain and frequency domain. The time domain carries out a time simulation of the response of the system to waves, current and a range of user-defined inputs. The frequency domain carries out linear frequency domain analysis of the response of the system to waves, current and a range of user-defined inputs. any nonlinearities present are approximated to be linear. It uses the result of the static analysis as the system's configuration at which to generate linear transfer functions that map the some underlying stochastic environmental (e.g. the wave elevation) or loading process to the system's response process.

In the following chapter, Chapter 5, the results from the dynamic analysis are presented. It presents graphs and numbers in regards to minimum effective tension, minimum effective top tension, maximum upper and lower flex joint angles, and the maximum von Mises stresses for the different materials and loading scenarios.

Chapter 5

Dynamic Simulation Results

In this chapter the simulation results from the OrcaFlex model presented in Chapter 4 are shown, with a main emphasis on the minimum effective tension, minimum effective top tension, maximum upper and lower flex joint angles, and the maximum von Mises stress in the riser.

In order to illustrate opportunities and limitations provided by application of lighter alternative riser materials, all the simulations are performed using the material properties of steel, aluminum and titanium. Three different main wave loadings are established; 7 m, 11.8 m, and 14.3 m wave heights H with corresponding periods T. To get an opinion on how the drilling fluid density influence the results, two different densities are used, namely 1025 kg/m^3 and 1500 kg/m^3. The simulations are performed for various tensioner settings. The tension in each tensioner starts at 300 kN and increases with 150 kN up to 1950 kN for each simulation. For steel risers the model collapsed with tensioner settings below 450 kN, thus, in that case the lowest tensioner setting was 450 kN.

5.1 Minimum Effective Tension

In order to ensure the stability of the riser and avoid buckling and collapse, a minimum tension setting is required. The effective tension should always be kept positive in all parts of the riser, even if a tensioner should fail. The riser is said to be in compression if the tension is negative. In most cases, the minimum effective tension is encountered at the bottom of the riser, which was the case in these simulations as well.

The results from the simulations are shown in graphs below. The horizontal axis on the graphs show the tensioner setting for each of the four tensioners, and the vertical axis shows the minimum effective tension the riser experience at the lower most section.

The results show that the minimum effective tension occurs at seabed. Not surprisingly, the results also show that the effective tension increases with increased top tension from the tensioners. In addition to the applied tension, the wave height and drilling fluid density has a significant influence on the minimum effective riser tension.

Increased wave height causes great fluctuations in the effective tension, this can bee seen in the graphs below and in the graphs in Appendix A.1, which shows the maximum effective tension. The drilling fluid also plays a major role when it comes to minimum effective tension. The applied top tension needs to be greater with heavier drilling fluid to keep the entire riser in tension.

When compering the results from the different materials, it can be concluded that the lighter materials are not as dependent on high top tension as the steel riser. Aluminum, due to its low weight, requires the lowest tensioner settings to be kept in continuous tension. Titanium requires the second lowest tension.

5.1.1 Steel Riser

Fig. 5.1 shows the minimum effective tension at seabed for steel riser filled with drilling fluid with density equal to sea water (1025 kg/m^3). While Fig. 5.2 shows the minimum effective tension at seabed for steel riser filled with 1500 kg/m^3 heavy drilling fluid.

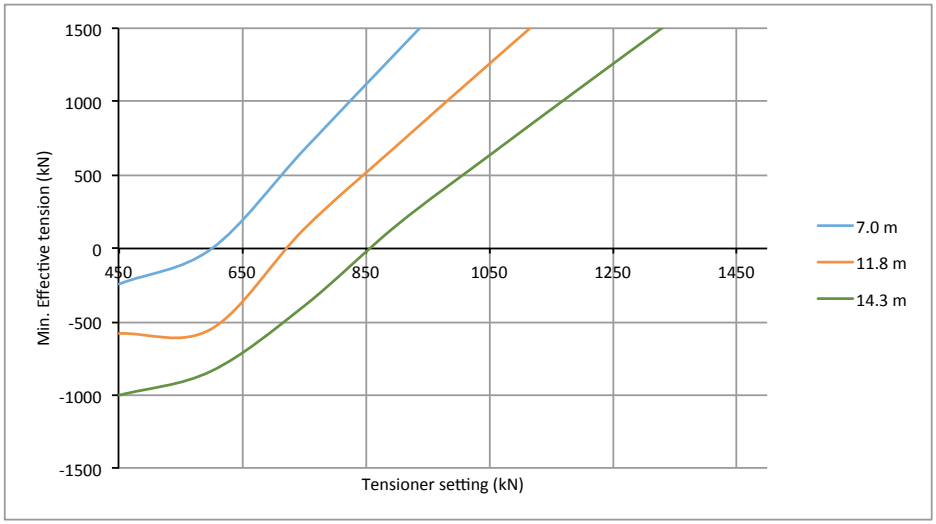

Fig. 5.1. Min. Effective tension at seabed, steel, drilling fluid density = 1025kg/m^3

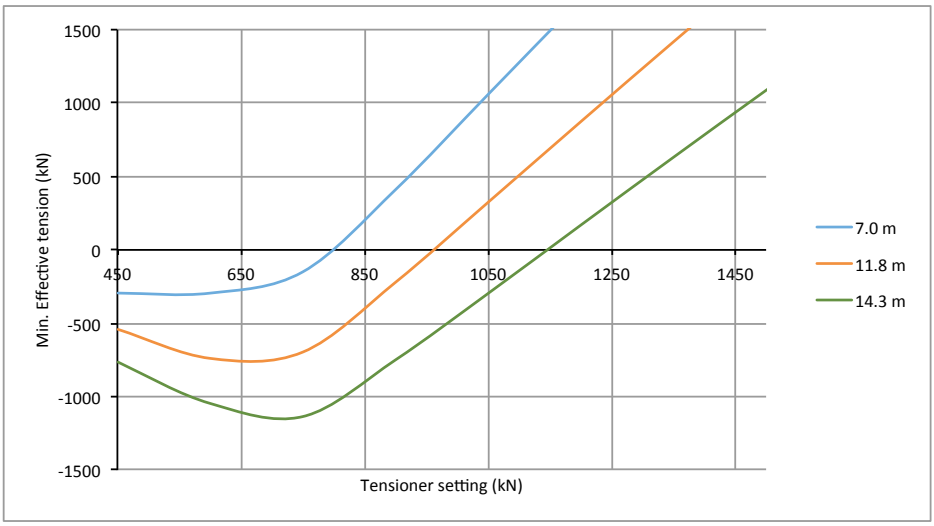

Fig. 5.2. Min. Effective tension at seabed, steel, drilling fluid density = 1500kg/m^3

5.1.2 Aluminum Riser

Fig. 5.3 shows the minimum effective tension at seabed for aluminum riser filled with drilling fluid with density equal to sea water (1025 kg/m^3). While Fig. 5.4 shows the minimum effective tension at seabed for aluminum riser filled with 1500 kg/m^3 heavy drilling fluid.

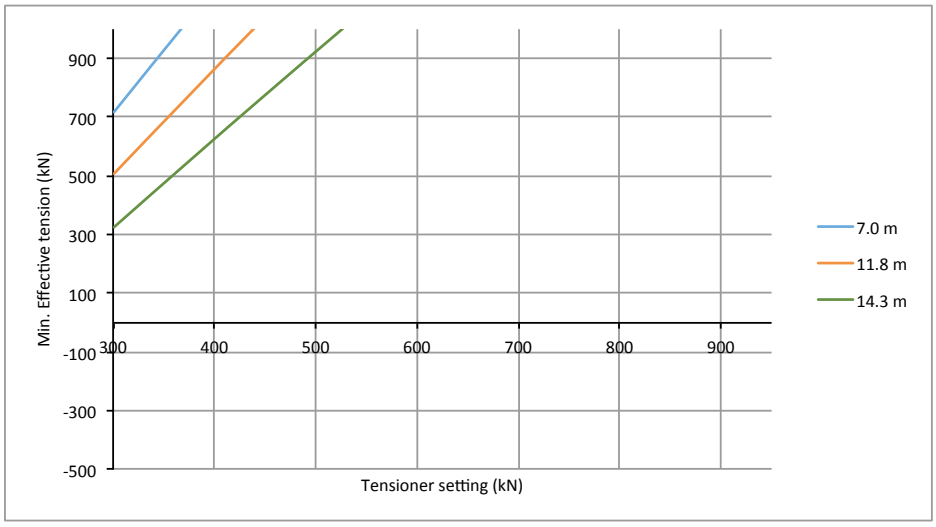

Fig. 5.3. Min. Effective tension at seabed, aluminum, drilling fluid density = $1025kg/m^3$

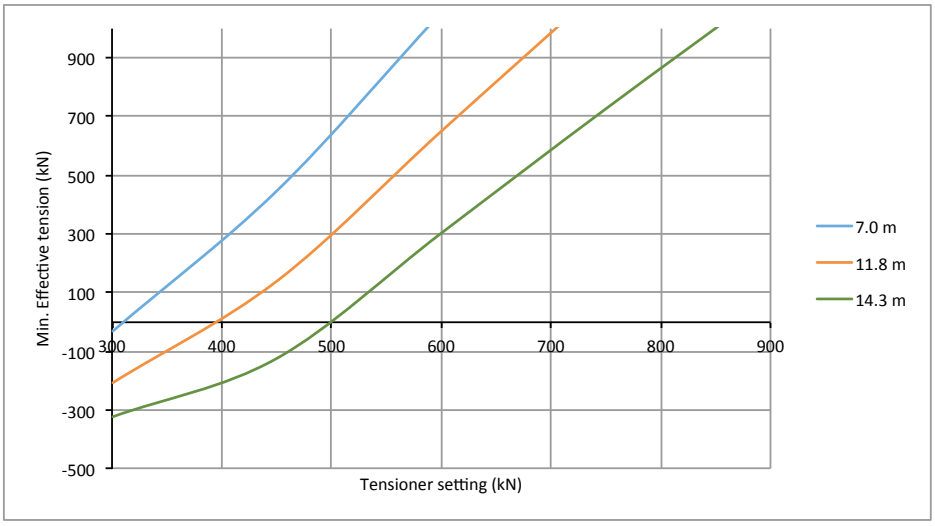

Fig. 5.4. Min. Effective tension at seabed, aluminum, drilling fluid density = $1500kg/m^3$

5.1.3 Titanium Riser

Fig. 5.5 shows the minimum effective tension at seabed for titanium riser filled with drilling fluid with density equal to sea water (1025 kg/m^3). While Fig. 5.6 shows the minimum effective tension at seabed for titanium riser filled with 1500 kg/m^3 heavy drilling fluid.

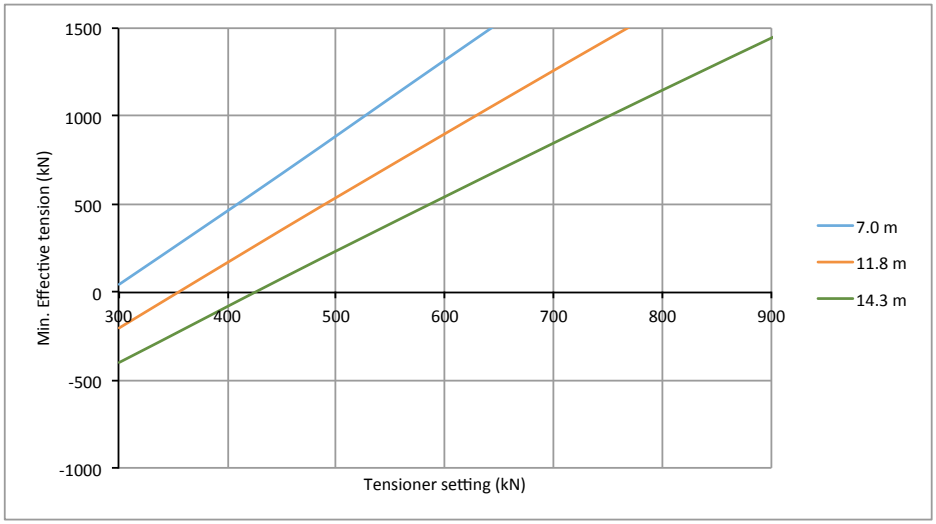

Fig. 5.5. Min. Effective tension at seabed, titanium, drilling fluid density = 1025kg/m^3

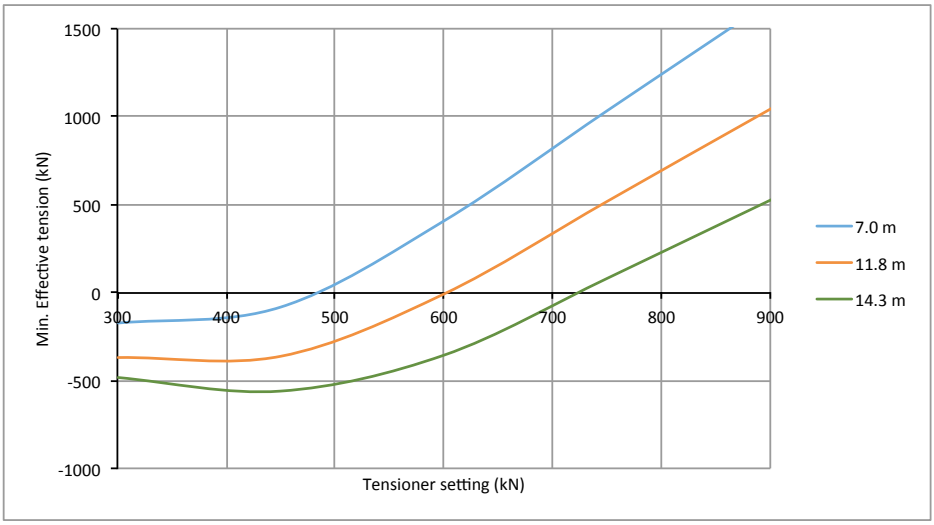

Fig. 5.6. Min. Effective tension at seabed, titanium, drilling fluid density = 1500kg/m^3

5.2 Minimum Effective Top Tension

In the section above the tensioner settings needed to keep the different risers in continuous tension was found. API RP 16Q and ISO 13624 uses Eg. 2.1 and Eq. 2.2 to determine minimum top tension T_{min} and minimum slip ring tension T_{SRmin}, respectively. In the calculations of the latter the submerged weight tolerance f_{wt} is set to 1.05 (not accurately weighted), the buoyancy loss and tolerance factor f_{bt} is set to the maximum value of 0.96, the reduction factor R_f, which relates vertical tension at the slip ring to tensioner setting to account for fleet angle and mechanical efficiency, is set to 0.95, and the number of tensioners subject to sudden failure n is set to the minimum of one. All the aforementioned values are obtained from the presented standards [2, 11]. The results from the calculations are shown in Table 5.1. Input and approach to these numbers can be found in Appendix A.2

Table 5.1. Minimum top tension determined by Eq. 2.1

Material	**dm** (kg/m^3)	**Tmin** (kN)
Steel	1025	6892
	1500	8391
Aluminum	1025	1749
	1500	3248
Titanium	1025	3526
	1500	5025

The results from the simulations are shown in graphs below. The horizontal axis on the graphs show the tensioner setting for each of the four tensioners, and the vertical axis shows the minimum effective top tension in the riser. The red lines are the theoretical minimum top tension values from Table 5.1.

The results show that the waves and drilling fluid density has an impact on the effective top tension. The highest waves gives the lowest minimum effective top tension, leading to an increase in required tensioner settings. When the drilling fluid density increases the T_{min} from the standards increase as well. The difference between the different drilling fluid density is greatest with low tensioner settings, for the higher tensioner settings the minimum effective tension is approximately the same.

It is interesting to compare these results with the required tensioner settings to keep the riser in continuous tension, which is found in the previous section. The latter is significantly lower than the suggested T_{min} obtained from the standards.

Also these results favors the aluminum riser, in terms of required tensioner settings to keep it above the limit, closely followed by titanium.

5.2.1 Steel Riser

The minimum effective top tension for a steel riser at different wave loadings are shown in Fig. 5.7 for drilling fluid density equal to 1025 kg/m^3 and in Fig. 5.8 for drilling fluid density equal to 1500 kg/m^3.

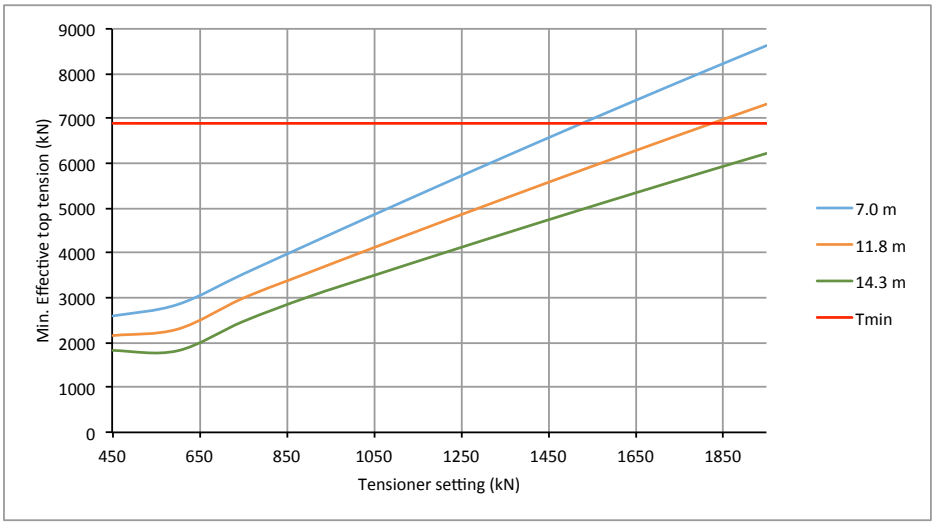

Fig. 5.7. Min. Effective top tension, steel, drilling fluid density = 1025kg/m^3

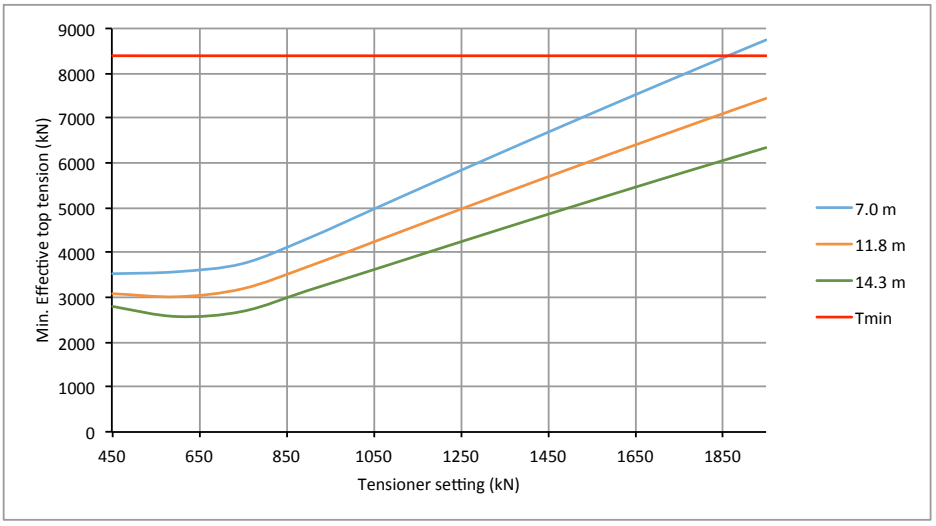

Fig. 5.8. Min. Effective top tension, steel, drilling fluid density = 1500kg/m^3

5.2.2 Aluminum Riser

The minimum effective top tension for a aluminum riser at different wave loadings are shown in Fig. 5.9 for drilling fluid density equal to 1025 kg/m^3 and in Fig. 5.10 for drilling fluid density equal to 1500 kg/m^3.

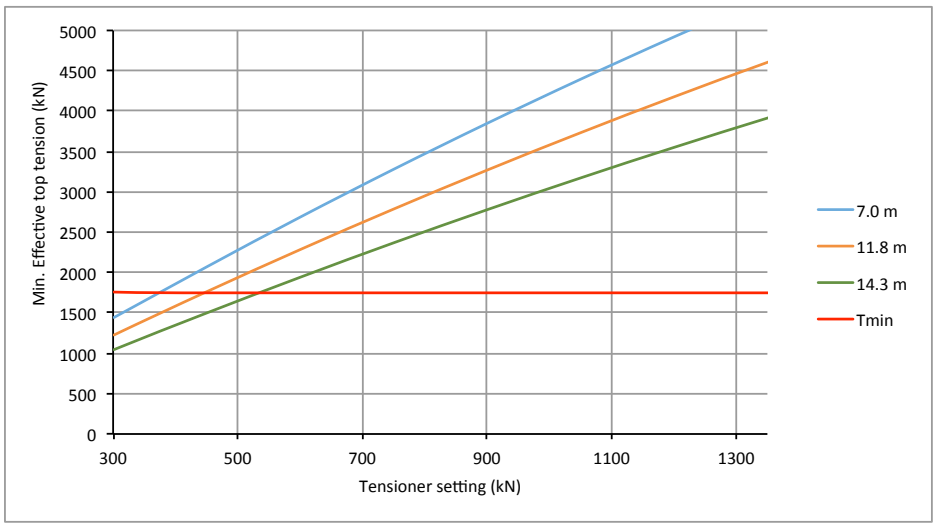

Fig. 5.9. Min. Effective top tension, aluminum, drilling fluid density = 1025kg/m^3

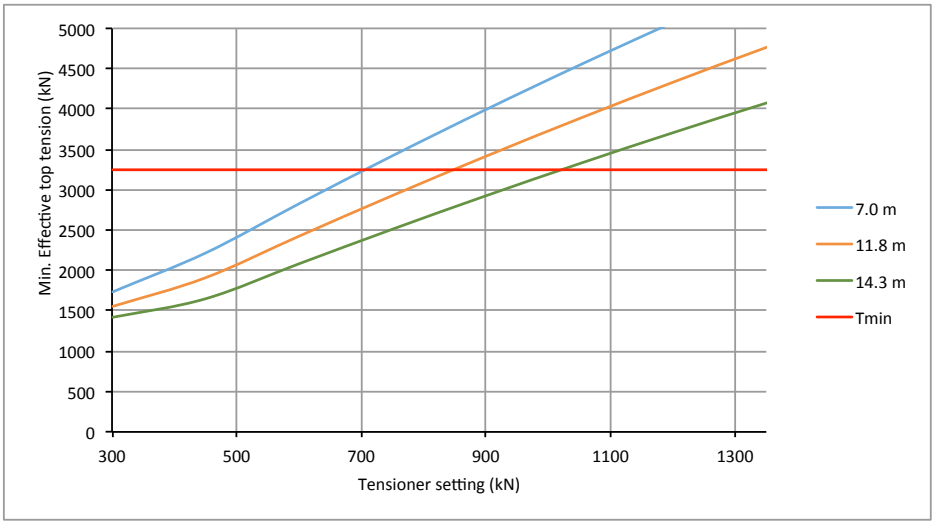

Fig. 5.10. Min. Effective top tension, aluminum, drilling fluid density = 1500kg/m^3

5.2.3 Titanium Riser

The minimum effective top tension for a titanium riser at different wave loadings are shown in Fig. 5.11 for drilling fluid density equal to 1025 kg/m^3 and in Fig. 5.12 for drilling fluid density equal to 1500 kg/m^3.

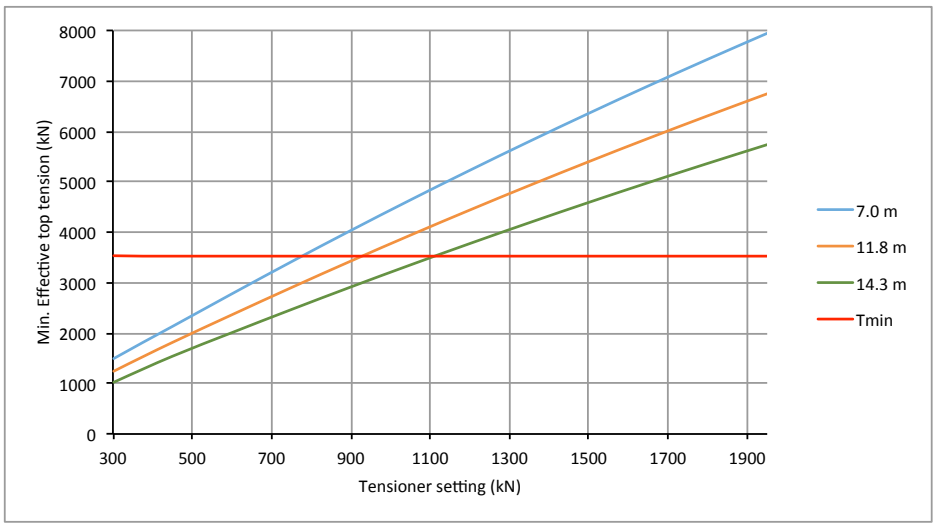

Fig. 5.11. Min. Effective top tension, titanium, drilling fluid density = 1025kg/m^3

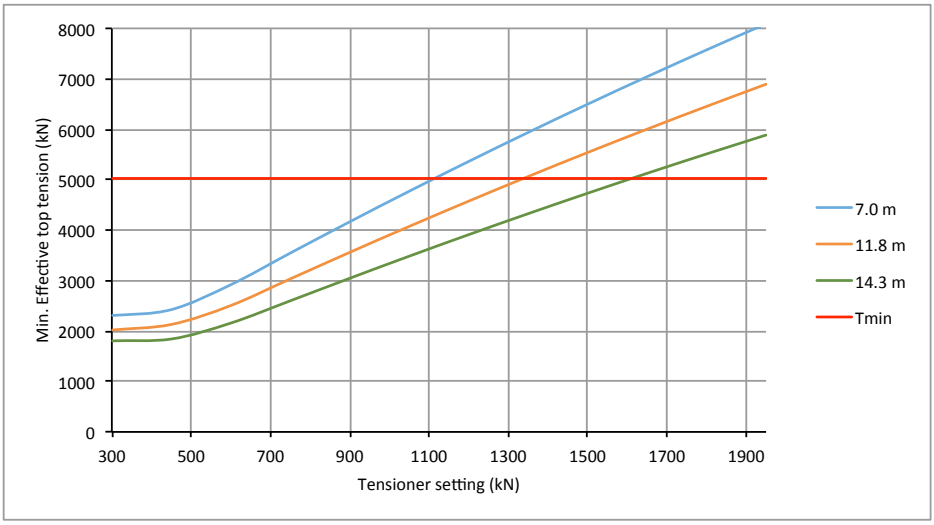

Fig. 5.12. Min. Effective top tension, titanium, drilling fluid density = 1500kg/m^3

5.3 Maximum Upper Flex Joint Angles

To summarize, the main function of the upper flex joint is to allow for the motion of the rig (described in Chapter 2), thereby reducing the stresses in the riser. The operational procedure should strive to maintain these angles as small as possible. The mean value 1.0-1.5 degrees and maximum value 5.0 degrees from the ISO standard should be considered as upper bounds.

Appendix A.3 shows the maximum upper flex joint angles for the waves presented in Table 4.7. The tensioners in the OrcaFlex model varies for the different materials and drilling fluid densities, and are set to fulfill the requirements from Table 5.1. The maximum upper flex joint angles seems to increase with the wave height, especially for the aluminum riser. However, the angle peaks at 7 m waves, which can be due to resonance. The results in Fig. A.7 may be misleading, due to the different tensioner settings for the different materials. To exclude the influence from the different tensioner settings, the same settings have been used for all the three materials. The wave loadings used are from 7 m, 11.8 m, and 14.3 m waves.

The results are shown in graphs below. Where the horizontal axis on the graphs show the tensioner setting for each of the four tensioners, and the vertical axis shows the maximum upper flex joint angle. The dotted red line is the API maximum upper flex joint angle design parameter, while the solid red line is the ISO maximum upper flex joint angle design parameter, both presented in Chapter 2.

The factor, which plays the biggest role in terms of maximum upper flex joint angle, seems to be the applied tension. When the applied tension increases, the maximum angle decreases. The drilling fluid density also affects the maximum angle; higher mud weight contributes in a positive manner (not so much in the case of aluminum riser). The wave height does not seem to influence the angle significantly. However, also here the 7 m waves shows the highest angles, which can, as already mentioned, be caused by a type of resonance in that exact combination of wave height and period.

The lighter materials, aluminum and titanium, shows higher angles than the more conventional riser material, steel. Thus, they need more top tension to keep the angles below the upper bounds.

5.3.1 Steel Riser

The maximum upper flex joint angles are for steel risers with drilling fluid density equal to $1025 kg/m^3$ are shown in Fig. 5.13, and in Fig. 5.14 for steel risers with drilling fluid density equal to $1500 kg/m^3$.

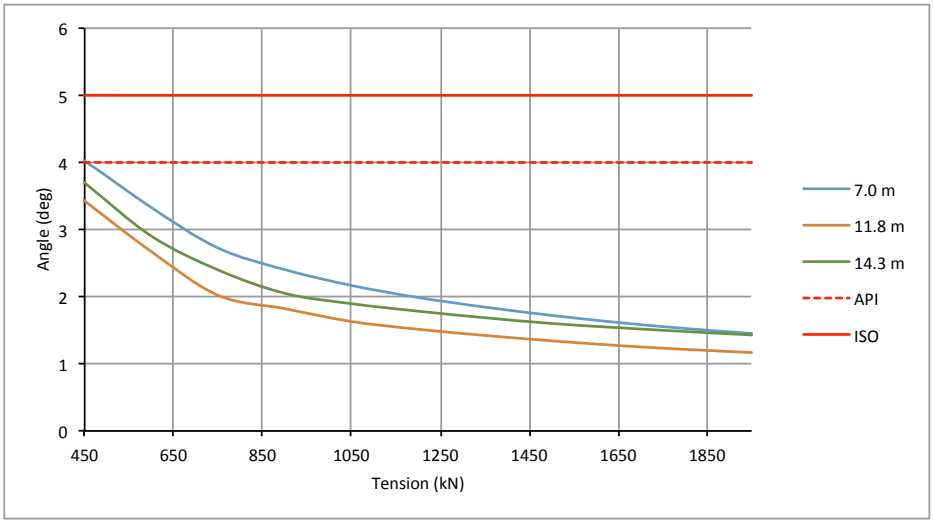

Fig. 5.13. Max. Upper flex joint angles, steel, drilling fluid density = $1025 kg/m^3$

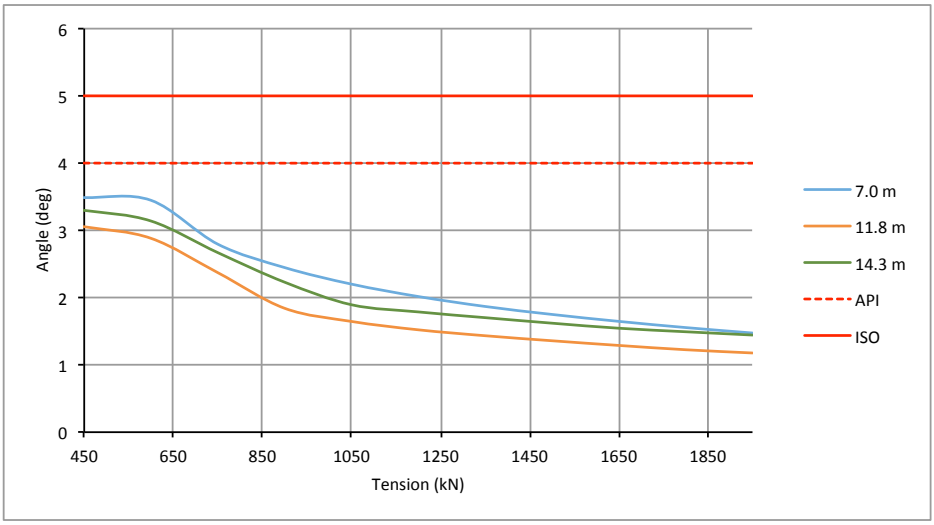

Fig. 5.14. Max. Upper flex joint angles, steel, drilling fluid density = $1500 kg/m^3$

5.3.2 Aluminum Riser

The maximum upper flex joint angles are for aluminum risers with drilling fluid density equal to $1025 kg/m^3$ are shown in Fig. 5.15, and in Fig. 5.16 for aluminum risers with drilling fluid density equal to $1500 kg/m^3$.

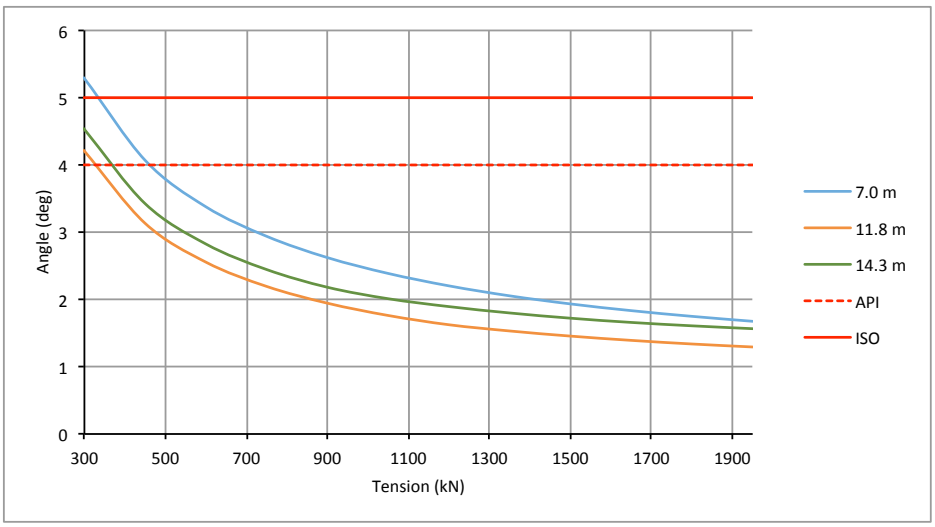

Fig. 5.15. Max. Upper flex joint angles, aluminum, drilling fluid density = $1025 kg/m^3$

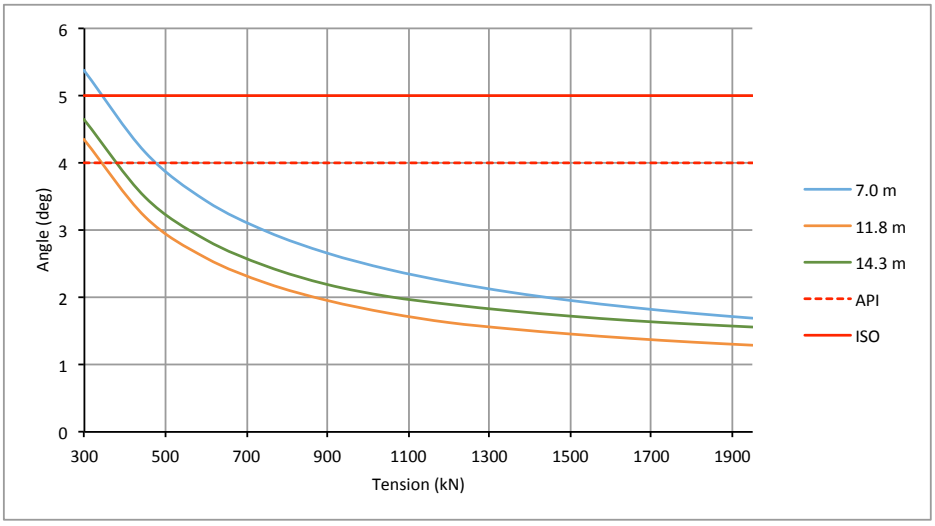

Fig. 5.16. Max. Upper flex joint angles, aluminum, drilling fluid density = $1500 kg/m^3$

5.3.3 Titanium Riser

The maximum upper flex joint angles are for titanium risers with drilling fluid density equal to $1025 kg/m^3$ are shown in Fig. 5.17, and in Fig. 5.18 for titanium risers with drilling fluid density equal to $1500 kg/m^3$.

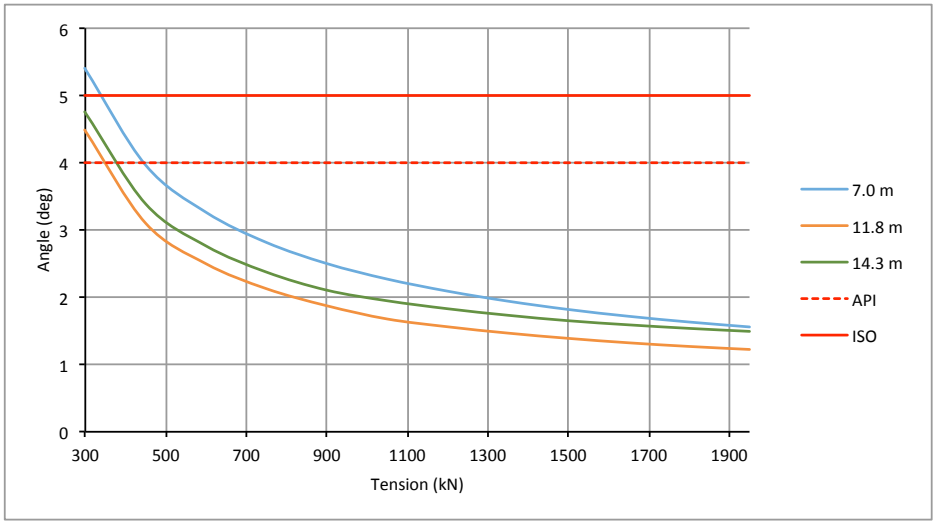

Fig. 5.17. Max. Upper flex joint angles, titanium, drilling fluid density = $1025 kg/m^3$

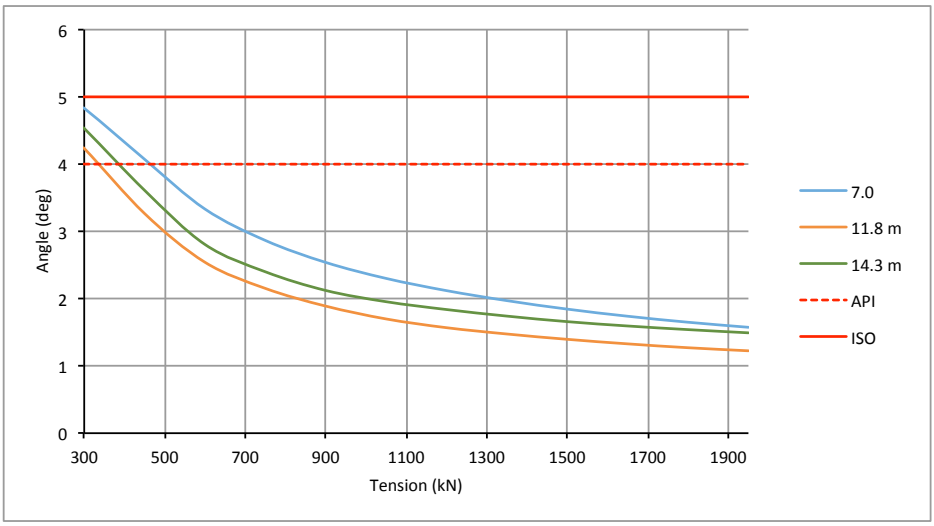

Fig. 5.18. Max. Upper flex joint angles, titanium, drilling fluid density = $1500 kg/m^3$

5.4 Maximum Lower Flex Joint Angles

The lower flex joint, which is part of the LMRP, is used to allow angular misalignment between the riser and the BOP stack, thereby reducing the stresses in the riser. The operational procedure should strive to maintain these angles as small as possible. The mean value 2.0 degrees and maximum value 5.0 degrees from the ISO standard should be considered as upper bounds.

Appendix A.3 shows the maximum lower flex joint angles for the waves presented in Table 4.7. The tensioners in the OrcaFlex model varies for the different materials and drilling fluid densities, and are set to fulfill the requirements from Table 5.1. The maximum lower flex joint angles seems to be unefected by the wave height, except from a small increase in angle at 7 m waves. The results in Fig. A.8 may be misleading, due to the different tensioner settings for the different materials. To exclude the influence from the different tensioner settings, the same settings have been used for all the three materials. The wave loadings used are from 7 m, 11.8 m, and 14.3 m waves.

The results are shown in graphs below. Where the horizontal axis on the graphs show the tensioner setting for each of the four tensioners, and the vertical axis shows the maximum lower flex joint angle. The dotted red line is the API maximum lower flex joint angle design parameter, while the solid red line is the ISO maximum lower flex joint angle design parameter, both presented in Chapter 2.

The graphs show that the lower flex joint angle is highly dependent on the applied tension. When the applied top tension is very low the riser might get in to compression at the bottom, which causes bending. The angles get even higher with increased drilling fluid density, this worsen the situation, and the required top tension to keep the lower flex joint angle below the upper bound increases. The waves seem to have the biggest impact on the angles when the applied tension is low. Then the highest waves give the highest angles.

The heavy steel riser is more prone to great lower flex joint angles, than the two lighter materials. It requires more top tension to stay below the upper bounds and to avoid getting in compression, which again can lead to bending and high angles at the bottom. Aluminum requires much less top tension to avoid the critical angles.

5.4.1 Steel Riser

The maximum lower flex joint angles are for steel risers with drilling fluid density equal to $1025 kg/m^3$ presented in Fig. 5.19, and in Fig. 5.20 for steel risers with drilling fluid density equal to $1500 kg/m^3$.

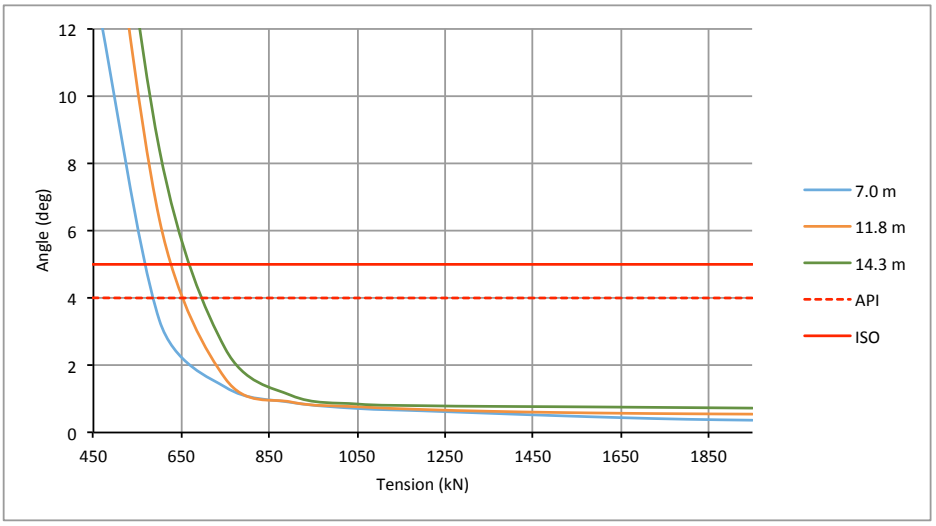

Fig. 5.19. Max. Lower flex joint angles, steel, drilling fluid density = $1025 kg/m^3$

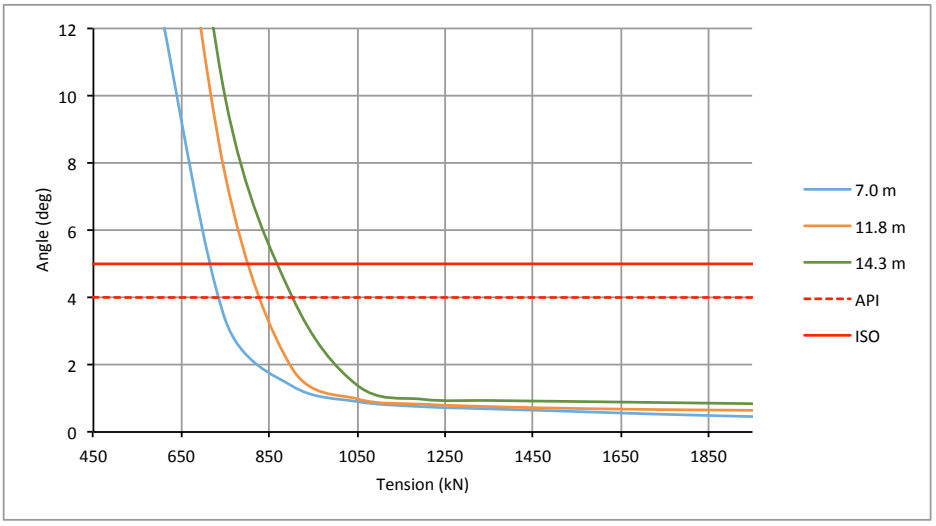

Fig. 5.20. Max. Lower flex joint angles, steel, drilling fluid density = $1500 kg/m^3$

5.4.2 Aluminum Riser

The maximum lower flex joint angles are for aluminum risers with drilling fluid density equal to $1025kg/m^3$ presented in Fig. 5.21, and in Fig. 5.22 for aluminum risers with drilling fluid density equal to $1500kg/m^3$.

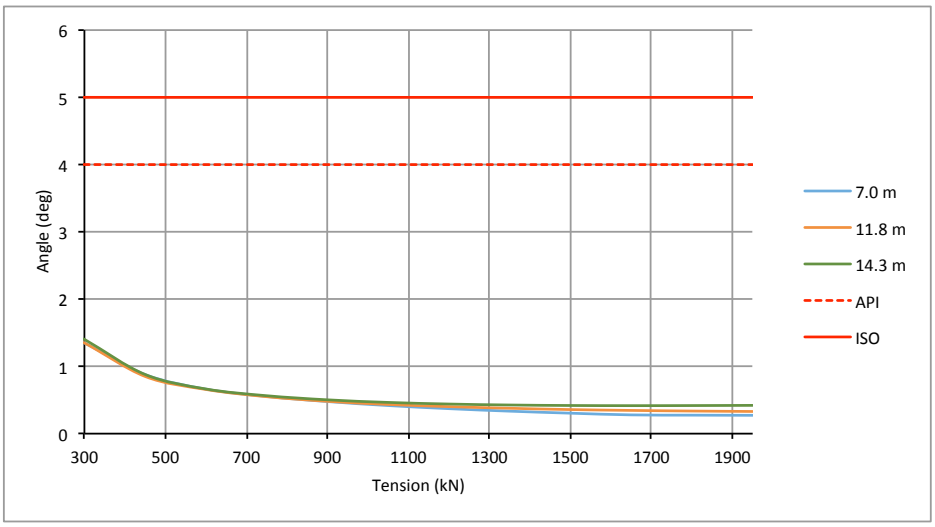

Fig. 5.21. Max. Lower flex joint angles, aluminum, drilling fluid density = $1025kg/m^3$

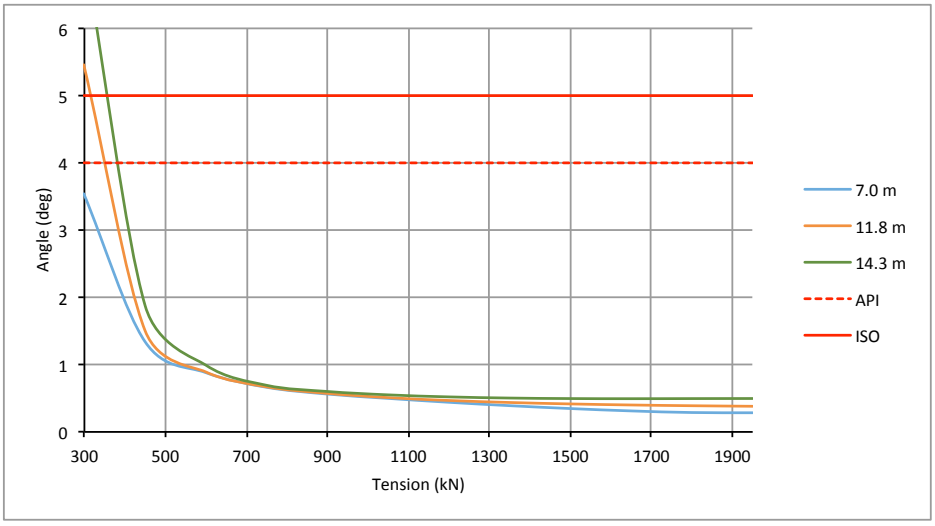

Fig. 5.22. Max. Lower flex joint angles, aluminum, drilling fluid density = $1500kg/m^3$

5.4.3 Titanium Riser

The maximum lower flex joint angles are for titanium risers with drilling fluid density equal to $1025 kg/m^3$ presented in Fig. 5.23, and in Fig. 5.24 for titanium risers with drilling fluid density equal to $1500 kg/m^3$.

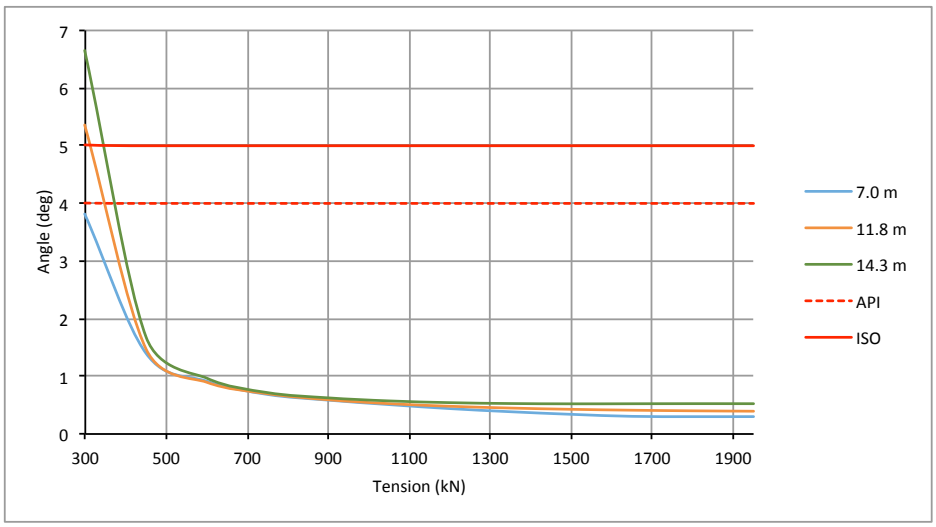

Fig. 5.23. Max. Lower flex joint angles, titanium, drilling fluid density = $1025 kg/m^3$

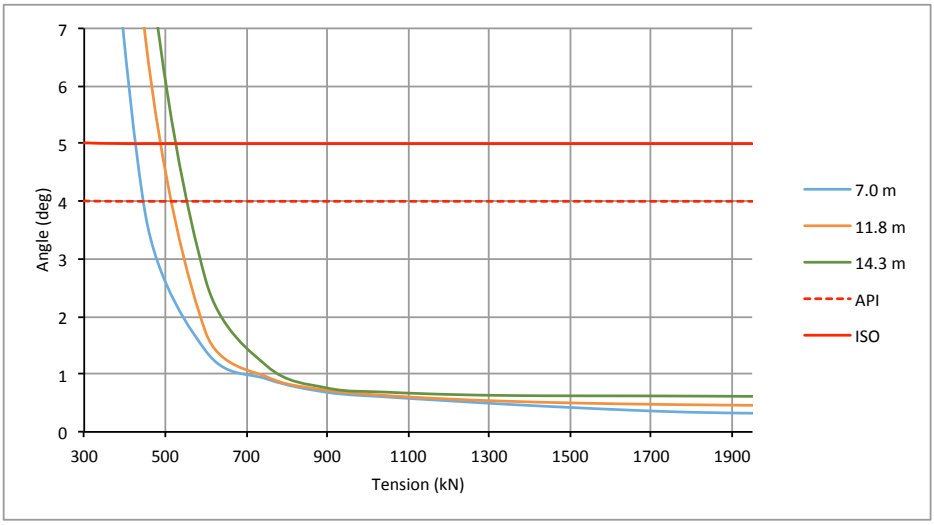

Fig. 5.24. Max. Lower flex joint angles, titanium, drilling fluid density = $1500 kg/m^3$

5.5 Maximum von Mises Stress

Looking at the effective stresses and maximum angles isolated, which have been done in the sections above, is not adequate in terms of getting the correct understanding and comparison of the different riser materials. von Mises is a criterion used to predict yielding of the riser during a combination of stresses produced by axial loads, bending, and pressure differences.

This section shows the results from the OrcaFlex simulations in graphs, where the horizontal axis is the tensioner setting for each of the four tensioners, and the vertical axis shows the maximum von Mises stress for different loading scenarios. The red line is the limit of allowable stress for the different materials, which is $0.67\sigma_y$ from the API and ISO standards. The limits are shown in Table 5.2.

Table 5.2. Yield and allowable stress

Parameter	Steel	Aluminum	Titanium
Yield strength (MPa)	560	350	483
Allowable stress (MPa)	375.2	234.5	323.61

The results in the graphs below show that the von Mises stress in the riser first decreases with increased top tension, before it at one point turns and starts to increase with increased top tension. This is probably due to the great bending and axial stresses observed in Appendix A.5 and A.6, respectively. These great bending stresses causes large lower flex joint angles observed in Section 5.4. The drilling fluid density on the other hand, seem to only have a noticeable effect on the maximum von Mises stress at lower tensioner settings.

At low tensioner settings the maximum von Mises stress is generated at the bottom of the riser, again due to the bending, while it on the other hand with maximum tension is generated at the surface, due to the high axial force from the tensioner system. This can bee seen in Appendix A.4.

5.5.1 Steel Riser

Fig. 5.25 and Fig. 5.26 shows the maximum von Mises stress for steel riser with drilling fluid density 1025 kg/m^3 and 1500 kg/m^3, respectively.

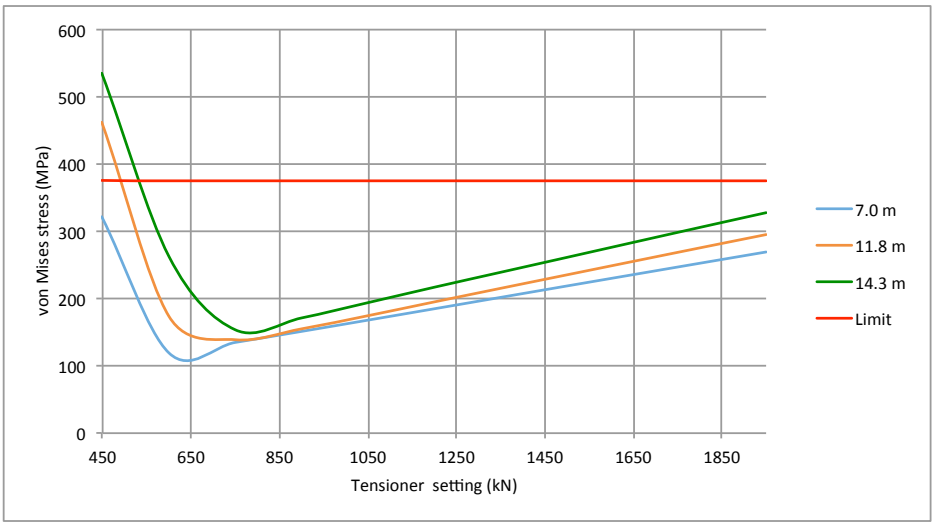

Fig. 5.25. Max. von Mises stress, steel, drilling fluid density = 1025kg/m^3

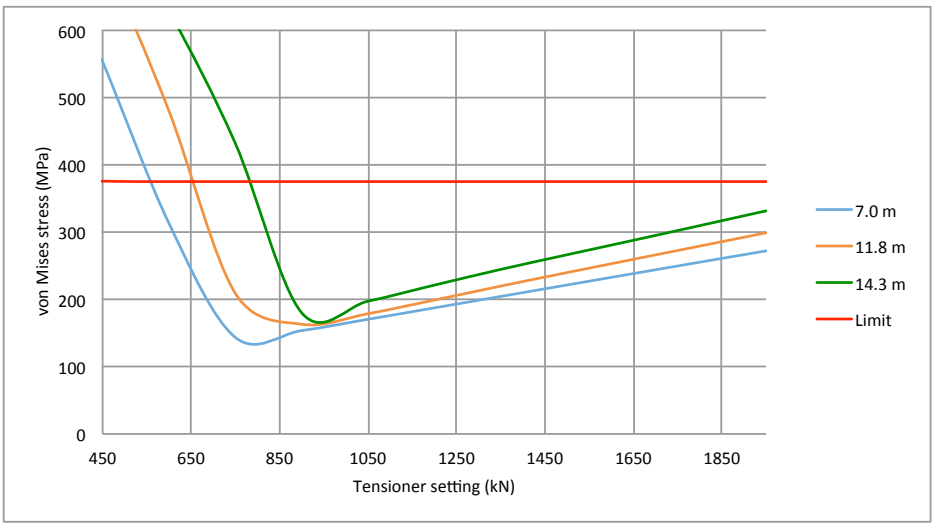

Fig. 5.26. Max. von Mises stress, steel, drilling fluid density = 1500kg/m^3

5.5.2 Aluminum Riser

Fig. 5.27 and Fig. 5.28 shows the maximum von Mises stress for aluminum riser with drilling fluid density 1025 kg/m^3 and 1500 kg/m^3, respectively.

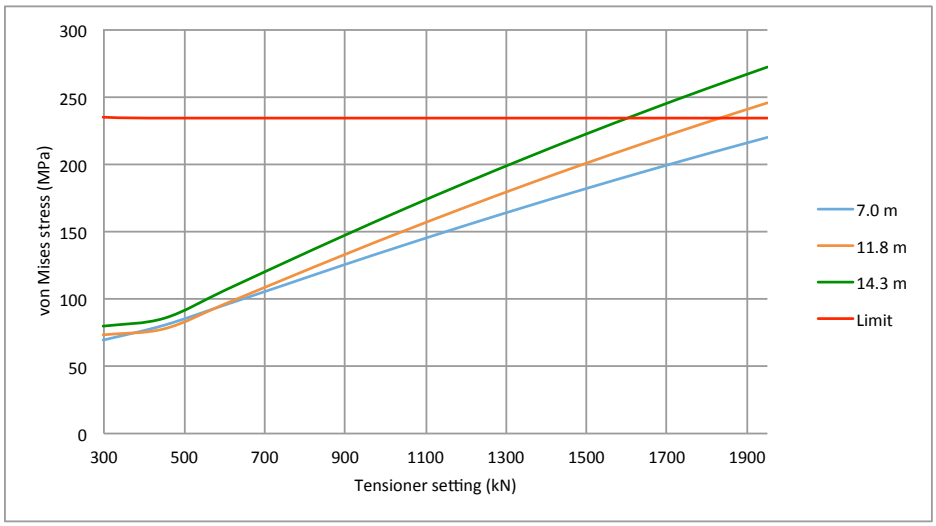

Fig. 5.27. Max. von Mises stress, aluminum, drilling fluid density = 1025kg/m^3

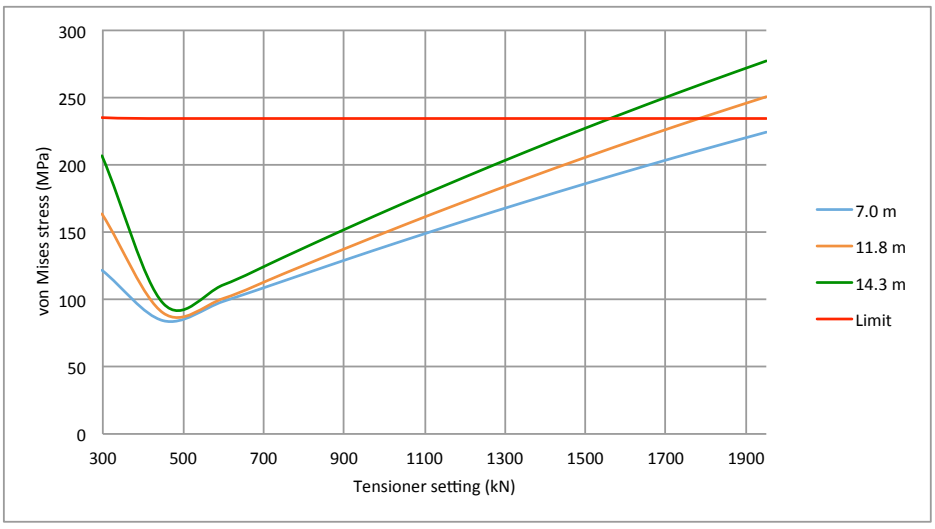

Fig. 5.28. Max. von Mises stress, aluminum, drilling fluid density = 1500kg/m^3

5.5.3 Titanium Riser

Fig. 5.29 and Fig. 5.30 shows the maximum von Mises stress for titanium riser with drilling fluid density 1025 kg/m^3 and 1500 kg/m^3, respectively.

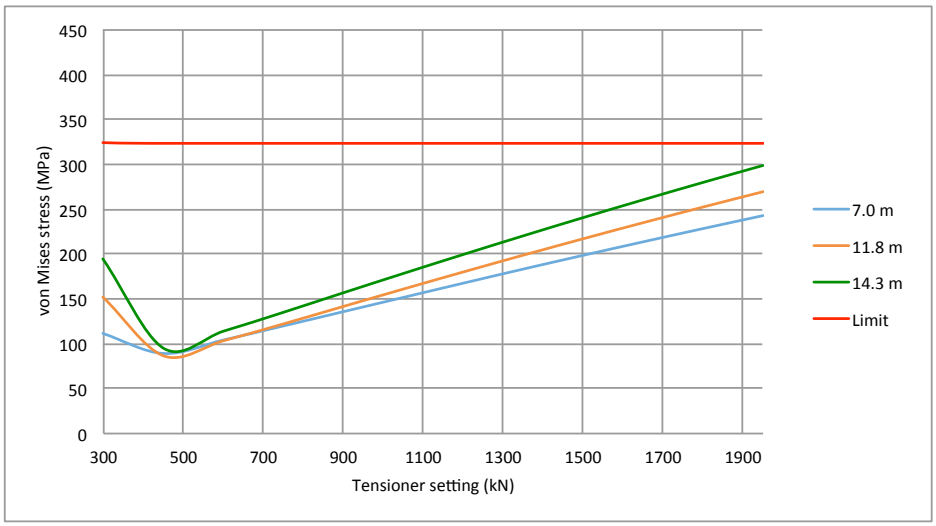

Fig. 5.29. Max. von Mises stress, titanium, drilling fluid density = $1025 kg/m^3$

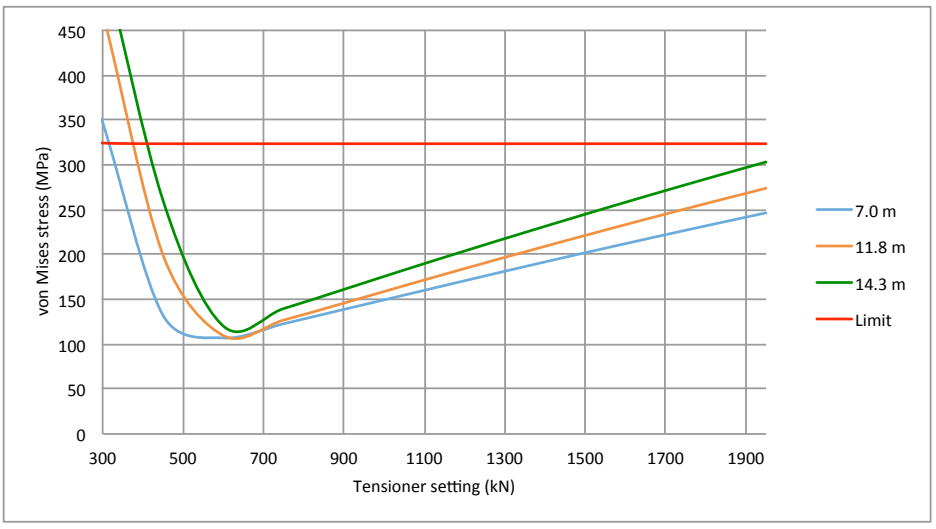

Fig. 5.30. Max. von Mises stress, titanium, drilling fluid density = $1500 kg/m^3$

Chapter 6

Summary and Discussion

This chapter summarize the results, discuss and try to explain the observed behavior of the different risers, based on the knowledge of fundamental mechanics and hydrodynamic loading.

6.1 Effect of Wave Height

The simulations have been performed with various design waves based on the information from the Aasta Hansteen field. The wave height and corresponding periods have been varied throughout the simulation, to determine the effect different waves have on the effective stresses, flex joint angles, and von Mises stresses.

The effective tension is highly influenced by the wave height, and both the minimum effective tension and maximum effective tension are observed at the highest waves (14.3 m). This creates great fluctuations in the effective tension and can cause fatigue in the riser and introduce fatigue promoting loads into the LMRP, the BOP stack and the hydraulic connectors.

The wave height seems to have a minor effect on the upper flex joint angles. However, when looking at the at the 7 m waves in Appendix A.3, there is an increase in angle. In discussion with supervisor the conclusion is that this peak in flex joint angle is generated by resonance in that exact combination of wave height and period.

The maximum lower flex joint angles are not very effected by the wave height, nor noteworthy of the resonance in the 7 m waves. It is nevertheless worth to mention that the difference in angle between the three different wave loadings (7, 11.8 and 14.3 m) is most noticeable when the applied top tension is low. Then the highest wave heights give the largest angles.

The wave height also influence the maximum von Mises stress. This is most noticeable at the lowest and highest top tension loadings. An increase in wave height will cause an increase in von Mises stress and the tensioners have a smaller "operational window" in terms of minimum and maximum applied top tension.

6.2 Effect of Drilling Fluid Density

All the simulations have been performed with two different drilling fluid densities. The lightest drilling fluid has the same density as sea water, which is 1025 kg/m^3, and the heavier drilling fluid has a density of 1500 kg/m^3. This has been done to determine the effect the density has on the effective stresses, flex joint angles, and von Mises stress.

When the drilling fluid density increases the internal hydrostatic pressure in the riser p_i increases. According to the effective tension theory presented earlier, an increase in internal pressure will decrease the effective tension. Since the pressure in the bottom is accordingly the highest, the effective tension at the bottom is most effected by drilling fluid density. Hence, to keep the entire riser in continuous tension, the required applied top tension increases with increased drilling fluid density. The results from the simulations show the same effect.

An increase in drilling fluid density does not influence the upper flex joint angle in a notable manner. However, for steel risers there is a slightly difference between the two densities. For lower tensioner settings there is a small drop in upper flex joint angles for the heaviest fluid. The two other materials are almost unaffected.

On the other hand, different drilling fluid densities heavily effect the lower flex joint angle. As mentioned, when the density increase the effective tension decreases. And at one stage the riser will be in compression, this leads to high bending loads on the riser at the bottom(See Appendix A.5). This bending causes large lower flex joint angles, which exceeds the recommended design limits.

von Mises stress is most effected by the drilling fluid density when the tensioner settings are low in terms of applied top tension. Then, an increase in density increase the von Mises stress. This is probably due to the extra bending stresses that occur at lower tensioner settings. At higher tensioner settings the von Mises stress is almost unaffected by the different densities.

6.3 Effect of Applied Top Tension

As mentioned, the riser is kept in tension by a tensioner system. This system applies a top tension to the tensioner ring. In this simulation model the system consists of four tensioners. Each tensioner is modelled with a specific tensioner setting; this setting is varied throughout the simulation. The main observation from the simulations is that the tensioner settings for the four tensioners plays a major role in terms of the effective tension, flex joint angles and von Mises stress.

The applied top tension will off course affect the effective tension in the riser. The effective tension increases almost linearly with increased top tension. Where the increase is not linear, there are other factors affecting the effective tension, such as large flex joint angles. In the simulation results, the minimum effective tension at seabed has been presented. Here the tensioner settings needed to keep the riser in tension are found for the different scenarios.

The minimum required top tension obtained from the simulation results are significantly lower than the minimum top tension T_{min} calculated from the ISO standard. This is probably due to the safety margin and that T_{min} applies even if a tensioner should fail.

None of the simulation results showed extreme upper flex joint angles, and most of them stayed below the upper bounds for all the different cases. However, the applied tension has a notable effect on the upper flex joint angle, and with increased upper tension the angle decreases.

The lower flex joint angle proves to be more critical than the former. When the applied top tension is low (depending on material) the angles exceeds the upper 5 °bound, defined by the ISO standard. In such situations, the applied top tension plays an important role and can be used to lower these angles and strive to maintain them as low as possible.

The von Mises stress is also highly effected by the applied top tension. For the majority of the cases, the maximum von Mises stress first decreases with increased top tension, before it at one point reaches a minimum value and starts to increase. This turn is in context of changing bending stresses (see Appendix A.5) and axial stresses (see Appendix A.4), as a result of changes in the effective tension (e.g. from compression to tension). The von Mises stress determines an upper limit for how much tension one can apply to the riser before the distortion energy exceeds the yield limit.

This upper limit can be called the maximum applied tension limit, and the tension needed to keep the riser in continuous tension can be called the minimum applied

tension. These limits create a window, which the tensioners need to stay inside to meet all the requirements.

The simulations performed in this thesis only simulated tensioners in the interval of 300 kN to 1950 kN. Due to this, the maximum values were not exceeded for all the scenarios. The limiting conditions for the minimum tension are determined from the simulation results to be the minimum effective tension (when T_{min} from ISO is excluded), while the maximum tension is determined by the maximum von Mises stress.

In Table 6.1 the minimum and maximum tension limits are presented. The maximum values written in italics for steel and titanium are estimated values from the graphs. These values are obtained from the the worst case scenarios, which turned to be 14.3 m waves and drilling fluid density = 1500 kg/m^3.

Table 6.1. Max. and Min. Tension boundaries

Type	**Min. Tension** (kN)	**Max. Tension** (kN)
Steel	1140	*2250*
Aluminum	500	1560
Titanium	725	*2100*

Below, the tensioner window is calculated for the different materials. Titanium proves to be the material with the biggest tensioner window.

$$T_{max} - T_{min} = T_{window} \tag{6.1}$$

$$Steel : (2250 - 1140)kN = 1110kN$$

$$Aluminium : (1560 - 500)kN = 1060kN$$

$$Titanium : (2100 - 725)kN = 1375kN$$

6.4 Application of Alternative Materials

As the drilling activities extend into deeper waters and harsher environments the attention has turned to looking at application of lighter alternative materials. This thesis has examined the possibilities and limitations of using aluminum or titanium risers as substitutes to the conventional steel riser in the Norwegian Sea environment, more accurate the deep water area of the Aasta Hansteen field.

The simulations have proved the lighter materials to be good alternatives to the steel riser. With correct tensioner settings they fulfill the limits set by the ISO standard in every scenario. Both aluminum and titanium risers have several pros that could make them better alternatives then steel.

The most obvious benefit is the reduced weight obtained by replacing the heavy steel riser. This can reduce drilling rig construction costs by reducing rig equipment power requirements. The weight also influences transportation and storage of the riser joints. Steel risers are more dependent on buoyancy modules, these buoyancy modules takes a lot of space and are expensive to purchase.

As HPHT and sour reservoirs become more common, higher demands on corrosion resistance must be imposed. Both the alternative materials provide a higher overall corrosion resistance than steel. In the longer run, the high corrosion resistance can contribute to increase the life span of the riser and help prevent fatal incidents in terms of bursted riser due to pitting or stress corrosion cracking.

The lighter materials are not as dependent on high applied top tension to stay in continuous tension. Due to its low weight, aluminum requires least top tension, then titanium. This can reduce the cost and power requirements of expensive tensioner systems. See Fig. 6.1.

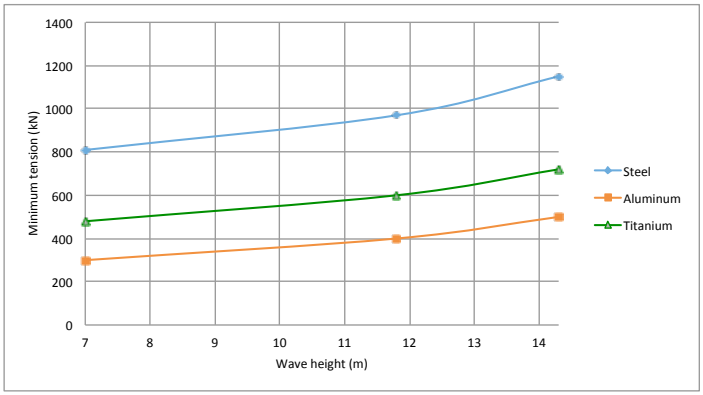

Fig. 6.1. Min. required applied top tension, drilling fluid density = $1500 kg/m^3$

Chapter 7

Conclusion

7.1 Concluding remarks

The concluding remarks of this thesis can be summarized in the following points:

- The wave height has a major impact on the effective tension, and can create great unwanted fluctuations in the effective tension. In addition, it influences the maximum von Mises stress in the riser. The upper and lower flex joint angles are not notable affected by the three different extreme wave heights. However, the upper angle seems to be affected by a sort of resonance at 7 m waves.
- The drilling fluid density influences the effective tension, and need to be considered when determining the required applied top tension to keep the entire riser in adequate tension. The upper flex joint angle is not influenced in a notable manner by the drilling fluid density. By contrast, it has a big influence on the lower flex joint angle, and need to be compensated by applied top tension to stay below the upper bound.
- The applied top tension plays a major role in terms of effective tension, upper and lower flex joint angles, and von Mises stresses. There exists an envelope where a safe operation window may be defined by the magnitude of the applied tension. To get a safe and adequate tensioner system this window should be prudently investigated during the design phase of the riser system.
- Aluminum and titanium have proved to fulfill all the given design parameters in the Norwegian Sea, and can potentially reduce the overall costs . Hence, should they both be considered as alternative materials to the conventional steel riser when weight is a concern.

7.2 Suggestions for future work

In order to improve the answer to the benefits and limitations in terms of applying lighter alternative riser materials, suggestions for future work follows:

- Since the tensioner settings proved to be such an important factor the modelling of these should be in close corporation with the supplier.
- The long term properties like corrosion and fatigue should be investigated.
- The loads and potential fatigue on the associated equipment (BOP, LMRP, connections and WH) should be investigated.
- To get the correct conclusion in terms of reduced costs, all the following points should be considered; potentially reduced time for handling and running, reduced wear and tear of rig equipment (due to less unit weight), reduced required equipment power, and reduced storage and transportation requirements.

References

[1] Allen, D. W. et al. (1998). Vortex-induced vibration of deepwater risers. In *Offshore Technology Conference*. Offshore Technology Conference.

[2] API (1993). Api rp 16q. *Recommended practice for design, selection, operation and maintenance of marine drilling riser systems*.

[3] Bai, Y. and Bai, Q. (2005). *Subsea pipelines and risers*. Elsevier.

[4] Blindheim, J., Rey, L., and Alexander, V. (1989). *Ecological features of the Norwegian Sea*.

[5] Boresi, A. P., Schmidt, R. J., and Sidebottom, O. M. (1993). *Advanced mechanics of materials*, volume 6. Wiley New York.

[6] DNV (2011). Loads on the drilling riser system.

[7] DNV, G. (2014). Dnv-rp-c205: Environmental conditions and environmental loads. *DNV GL, Oslo, Norway*.

[8] Greenburg, J. (2003). Different riser material compete for acceptance. *Drilling Contractor*, pages 30–31.

[9] Hariharan, M. and Thethi, R. (2007). Drilling riser management in deepwater environments.

[10] IEA (2016). World energy outlook 2016.

[11] ISO (2009). 13624-1:2009. *Part 1: Design and opertion of marine drilling riser equipment*.

[12] M. Gelfgat, V. Tikhonov, V. C. L. R. (2013). Lightweight riser experience - opportunities to overcome ultra-deep water challenges.

[13] Matrix (2014). Drilling riser buoyancy systems.

[14] MPE (2014). Facts, the norwegian petroleum sector. *Ministry of Petroleum and Energy, ISSN 1504-3398*.

[15] NPD (2017). Factpages norwegian petroleum directorate, aasta hansteen. *http://factpages.npd.no/factpages/Default.aspx?culture=en*.

[16] Orcina (2017). Orcaflex manual 2017.

[17] Sauer, C. W., Sexton, J. B., Sokoll, R. E., Thornton, J. M., et al. (1996). Heidrun tlp titanium drilling riser system. In *Offshore Technology Conference*. Offshore Technology Conference.

[18] Sengupta, P., Low, Y. M., Zhang, X., Adaikalaraj, P. F. B., and Koh, C. G. (2016). Reliability assessment of marine drilling risers with correlated random variables. In *ASME 2016 35th International Conference on Ocean, Offshore and Arctic Engineering*. American Society of Mechanical Engineers.

[19] Sparks, C. P. (2007). *Fundamentals of Marine Riser Mechanics*.

[20] Standard, N. (2007). Actions and action effects, n-003. *Oslo: Norwegian Technology Standards Institution*.

[21] Statoil (2013). Aasta hansteen field metocean design basis. *MBM-NKG-RA0023*.

[22] Trent, D. (2012). Tensioner system with recoil controls. US Patent 8,157,013.

[23] Veritas, D. N. (2002). Design of titanium risers.

[24] Yong Bai, Q. B. (2010). *Subsea Engineering Handbook*.

Appendix A

A.1 Maximum Effective Tension

Fig. A.1, Fig. A.2 and Fig. A.3 shows the maximum effective tension observed when looking at the entire riser length, for steel, aluminum, and titanium risers, respectively. The maximum effective tension occurs at the biggest waves.

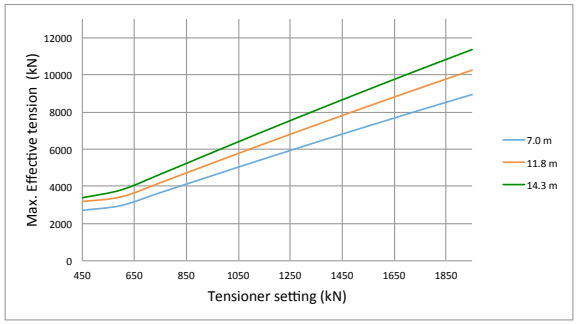

(a) Drilling fluid density = $1025 kg/m^3$

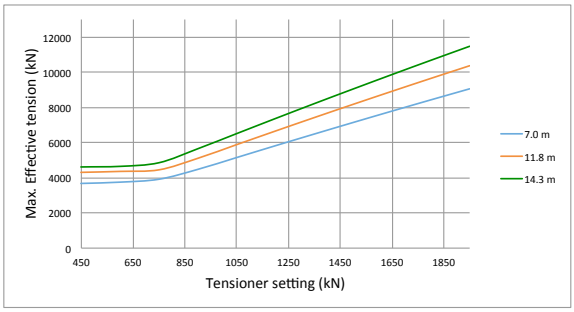

(b) Drilling fluid density = $1500 kg/m^3$

Fig. A.1. Max. Effective tension in steel riser

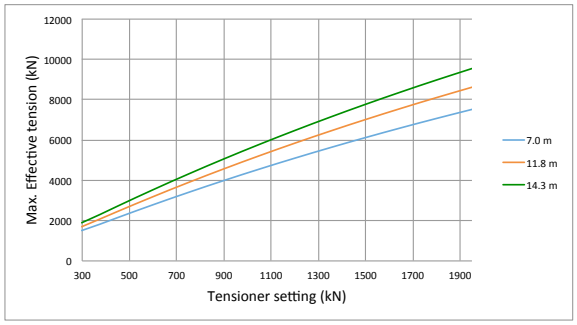

(a) Drilling fluid density = $1025 kg/m^3$

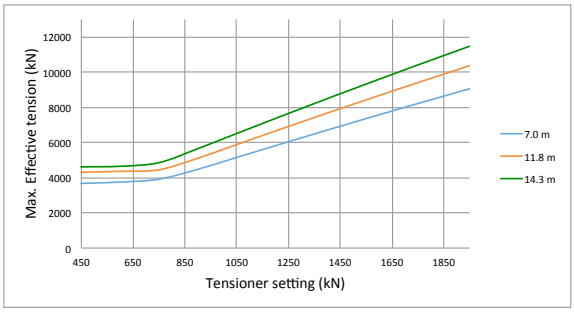

(b) Drilling fluid density = $1500 kg/m^3$

Fig. A.2. Max. Effective tension in aluminum riser

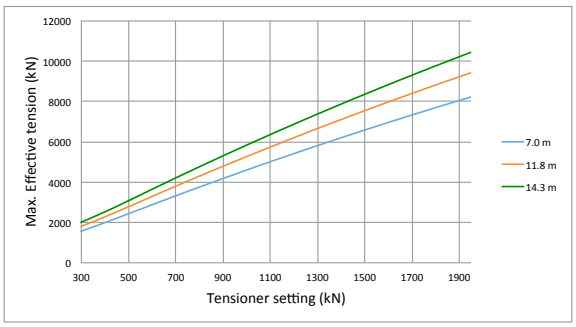

(a) Drilling fluid density = $1025 kg/m^3$

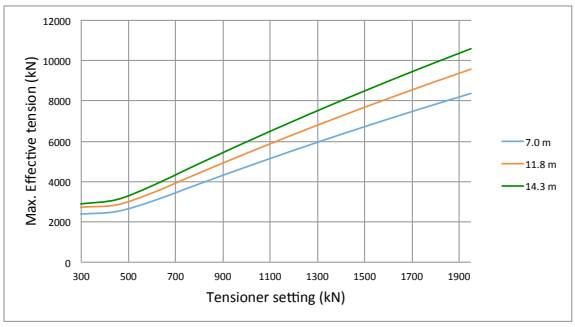

(b) Drilling fluid density = $1500 kg/m^3$

Fig. A.3. Max. Effective tension in titanium riser

Fig. A.4, Fig. A.5 and Fig. A.6 shows the maximum effective tension observed at the bottom of the riser, for steel, aluminum, and titanium risers, respectively. The maximum effective tension occurs at the biggest waves.

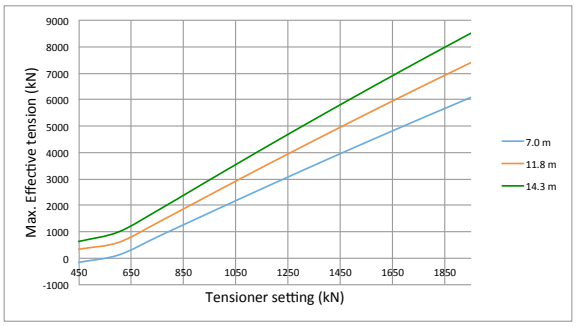

(a) Drilling fluid density = $1025 kg/m^3$

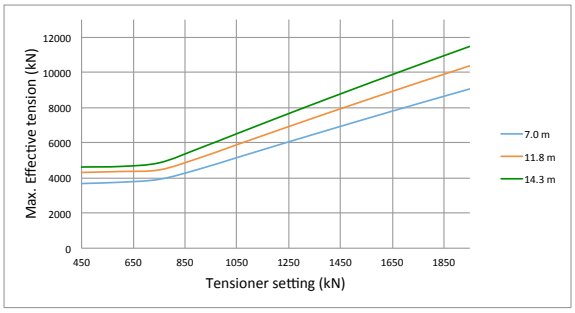

(b) Drilling fluid density = $1500 kg/m^3$

Fig. A.4. Max. Effective tension at seabed in steel riser

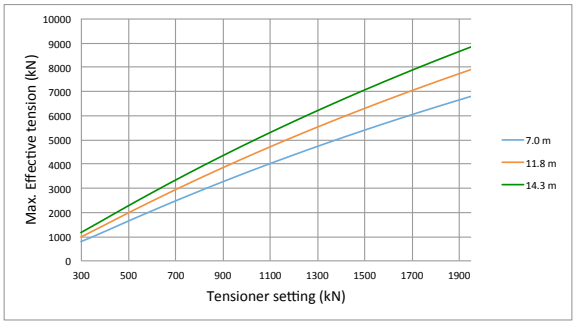

(a) Drilling fluid density = $1025 kg/m^3$

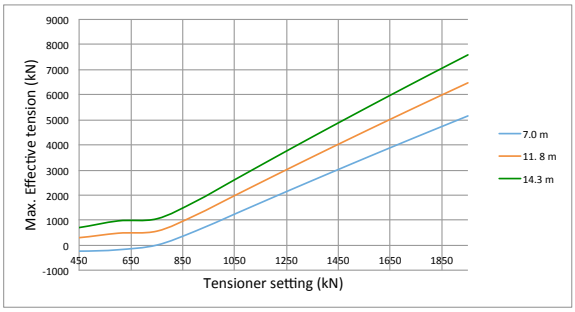

(b) Drilling fluid density = $1500 kg/m^3$

Fig. A.5. Max. Effective tension at seabed in aluminum riser

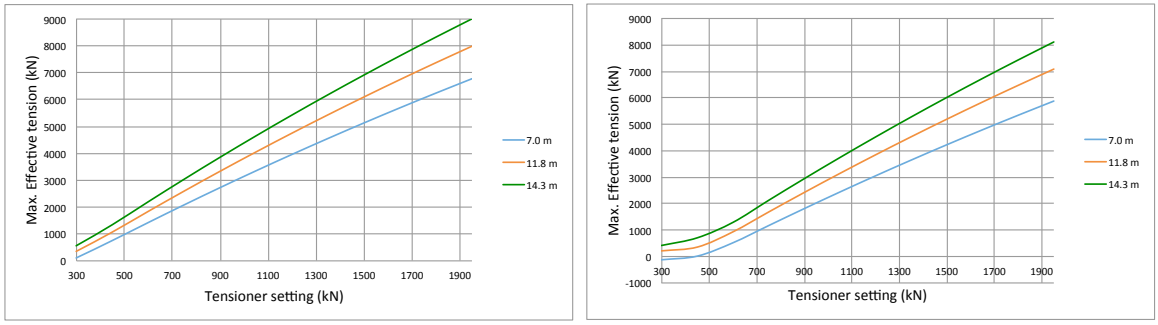

(a) Drilling fluid density = $1025 kg/m^3$ **(b)** Drilling fluid density = $1500 kg/m^3$

Fig. A.6. Max. Effective tension at seabed in titanium riser

A.2 Input and Calculations of Minimum Required Top Tension

The input parameters and minimum required top tension calculations described in Chapter 2.3 are presented in tables below.

Table A.1. Distances

Drilling Fluid Column to point of consideration	(m)	H_m	1219.30
Sea Water Column to point of consideration	(m)	H_w	1193.80
Height of LMRP + BOP	(m)	$H_{LMRP+BOP}$	8.50
Height of WH	(m)	H_{WH}	1.50
Distance from Tensioner Ring to MSL	(m)	H_{TR-MSL}	10.00
Height of Storm Surge + Tide	(m)	H_{SS+T}	3.80
Dinstance from RKB to MSL	(m)	$H_{RKB-MSL}$	27.50
Distance from RKB to Mud Line	(m)	H_{RKB-ML}	2.00

$$H_m = L_r - H_{TR-MSL} + H_{SS+T} + H_{RKB-MSL} - H_{RKB-ML}$$

$$H_w = WD - H_{LMRP+BOP} - H_{WH} + H_{SS+T}$$

Where WD is the water depth (1200 m).

Table A.2. Constants

Sea Water Density	(kg/m^3)	d_w	1025
Submerged Weight Tolerance Factor		f_{wt}	1.05
Buoyancy Loss and Tolerance Factor		f_{bt}	0.96
Reduction Factor		R_f	0.95
Net Lift of Buoyancy Material		B_n	0

Table A.3. Riser Data

Length	(m)	L_r	1200.00
Submerged Length	(m)	L_{rsub}	1190.00
Inner diameter	(m)	ID_r	0.489
Outer diamter	(m)	OD_r	0.533
Cross-sectional area	(m^2)	A_{csar}	0.03532
Number of Tensioners		N	4
Number of Tensioners subject to sudden failure		n	1
Steel density	(kg/m^3)	d_{rs}	7850
Aluminum density	(kg/m^3)	d_{ra}	2700
Titanium density	(kg/m^3)	d_{rt}	4480

$$L_{rsub} = L_r - H_{TR-MSL}$$

$$A_{csar} = \pi/4(OD_r^2 - ID_r^2)$$

Table A.4. Auxilary Lines Data

Length	(m)		1200.00
Sumberged Length	(m)		1190.00
Material density	(kg/m^3)		7850
Inner diameter	(m)	ID_a	0.1143
Outer diameter	(m)	OD_a	0.165
Cross-sectional area of one line	(m^2)	A_{csaa}	0.01112
Number of lines			2

$$A_{csaa} = \pi/4(OD_a^2 - ID_a^2)$$

Dry riser weight

$$Dryriserweight = L_r d_r (A_{csar} + A_{csaa})$$

$$Steel = 1200 * 7850 * (0.0353 + 0.0111) = 437088kg$$

$$Aluminum = 1200 * 2700 * (0.0353 + 0.0111) = 150336kg$$

$$Titanium = 1200 * 4480 * (0.0353 + 0.0111) = 249446kg$$

Table A.5. Output

Steel (7850 kg/m^3)				
Drilling fluid density	(kg/m^3)	dm	1025	1500
Submerged Riser Weight w/aux lines	(kg)	W_s	472015	472015
Minimum Slip Ring Tension	(kN)	T_{SRmin}	4910	5978
Minimum Required Top Tension	(kN)	T_{min}	6892	8391
Aluminum (2700kg/m^3)				
Drilling fluid density	(kg/m^3)	dm	1025	1500
Submerged Riser Weight w/aux lines	(kg)	W_s	116288	1116288
Minimum Slip Ring Tension	(kN)	T_{SRmin}	1246	3247959
Minimum Required Top Tension	(kN)	T_{min}	1749	3248
Titanium (4480 kg/m^3)				
Drilling fluid density	(kg/m^3)	dm	1025	1500
Submerged Riser Weight w/aux lines	(kg)	W_s	239238	239238
Minimum Slip Ring Tension	(kN)	T_{SRmin}	2512	3580
Minimum Required Top Tension	(kN)	T_{min}	3526	5025

$$W_s = (L_r A_{csar} d_r) - (L_{rsub} A_{csar} d_w) + (2L_r A_{csaa} d_r) - (2L_{rsub} A_{csaa} d_w)$$

$$T_{SRmin} = W_s f_{wt} - B_n f_{bt} + A_i[d_m H_m - d_w H_w]$$

$$T_{min} = \frac{T_{SRmin} N}{R_f (N - n)}$$

A.3 Maximum upper and lower flex joint angles

Fig. A.7 shows the maximum upper flex joint angles for the waves presented in Table 4.7. The tensioners in the OrcaFlex model varies for the different materials and drilling fluid densities, and are set to fulfill the requirements from Table 5.1. The maximum upper flex joint angles seems to increase with the wave height, especially for the aluminum riser. However, the angle peaks at 7 m waves, which can be due to resonance.

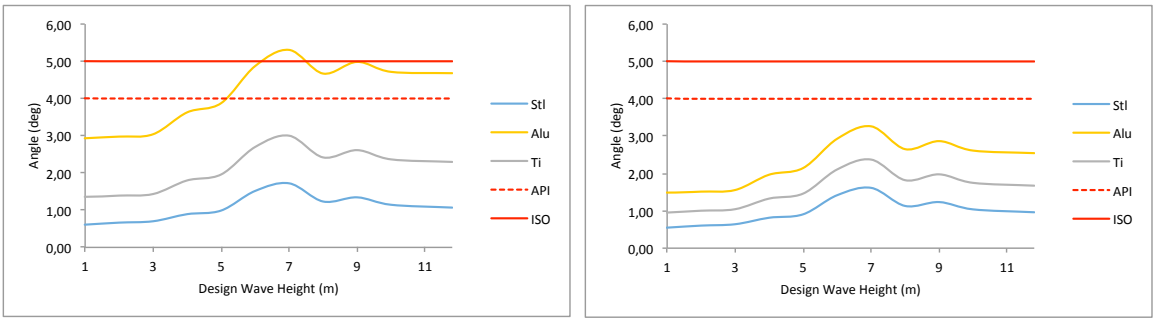

(a) Drilling fluid density = $1025 kg/m^3$ **(b)** Drilling fluid density = $1500 kg/m^3$

Fig. A.7. Max. upper flex jt. angle for various design waves

Fig. A.8 shows the maximum lower flex joint angles for the waves presented in Table 4.7. The tensioners in the OrcaFlex model varies for the different materials and drilling fluid densities, and are set to fulfill the requirements from Table 5.1. The maximum lower flex joint angles seems to be unefected by the wave height, except from a small increase in angle at 7 m waves.

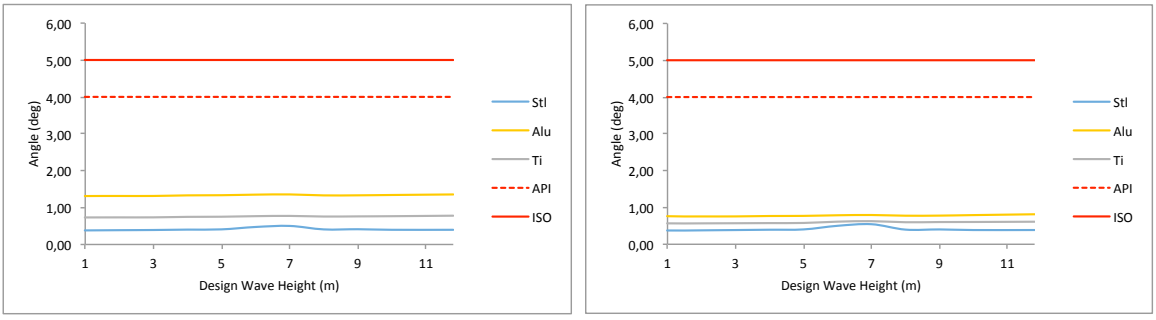

(a) Drilling fluid density = $1025 kg/m^3$ **(b)** Drilling fluid density = $1500 kg/m^3$

Fig. A.8. Max. lower flex jt. angle for various design waves

A.4 Maximum von Mises Stress

Fig. A.9 shows the maximum von Mises stress through the entire length of the riser, from surface down to seabed. The tensioner settings are set to the lowest and highest values simulated. The graphs show that; at low tensioner settings the maximum von Mises stress is generated at the bottom of the riser, again due to the bending, while it on the other hand with maximum tension is generated at the surface, due to the high axial force from the tensioner system.

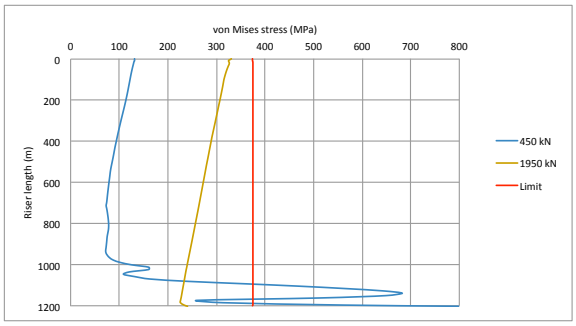

(a) Steel Riser

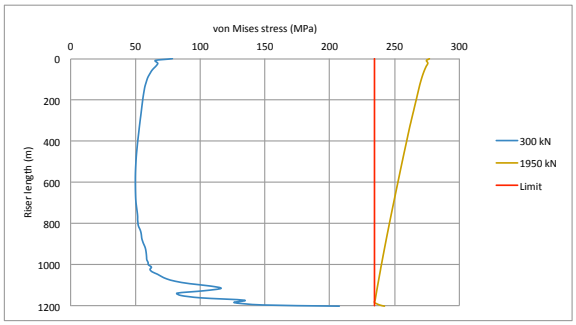

(b) Aluminum Riser

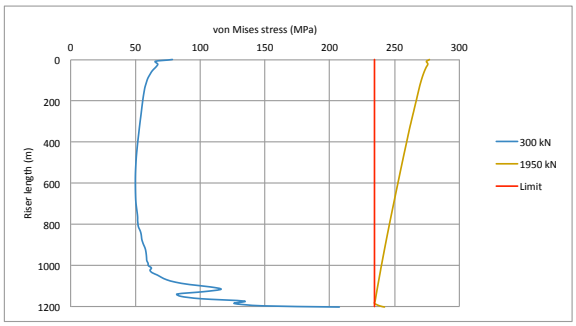

(c) Titanium Riser

Fig. A.9. Max. von Mises stress, drilling fluid density = $1500 kg/m^3$

A.5 Maximum Bending Stress

The graphs below show the maximum bending stresses occurring with 14.3 m waves and with drilling fluid density equal to 1500 kg/m^3. Fig. A.10 shows the absolute maximum bending stress in the riser with varying tensioner settings. The bending stresses decreases with increased applied top tension.

Fig. A.11a and A.11b show the maximum bending stress through the entire length of the riser, from surface down to seabed. The tensioner settings are set to the minimum in Fig. A.11a and maximum in Fig. A.11b. With low applied top tension the bending stress is most critical at the bottom, while for the higher top tension the bending stress is more evenly distributed.

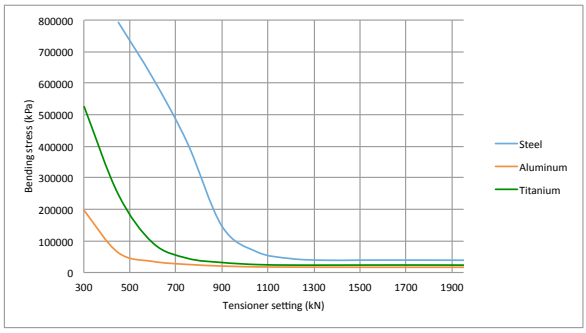

Fig. A.10. Max. Bending stress, drilling fluid density = $1500kg/m^3$

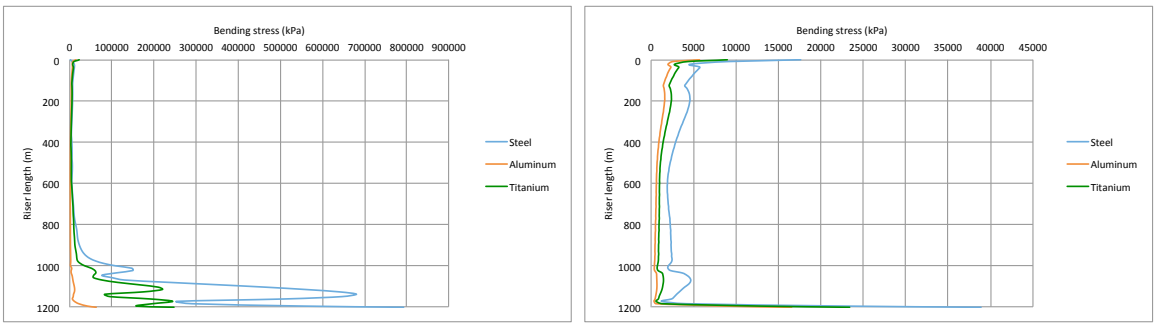

(a) 450 kN **(b)** 1950 kN

Fig. A.11. Max.Bending stress through the entire length of riser, drilling fluid density = $1500kg/m^3$

A.6 Maximum Axial Stress

The graphs below show the maximum axial stresses occurring with 14.3 m waves and with drilling fluid density equal to 1500 kg/m^3. Fig. A.12 shows the absolute maximum axial stress in the riser with varying tensioner settings. The axial stresses first decreases with increased applied top tension before it starts to slightly increase.

Fig. A.13a and A.13b show the maximum axial stress through the entire length of the riser, from surface down to seabed. The tensioner settings are set to the minimum in Fig. A.13a and maximum in Fig. A.13b. With low applied top tension the axial stress increases with depth and is worst at the bottom. For the higher top tension the axial stress decreases with depth.

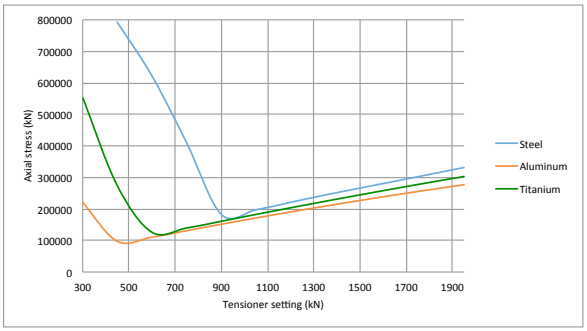

Fig. A.12. Max. Axial stress, drilling fluid density = $1500kg/m^3$

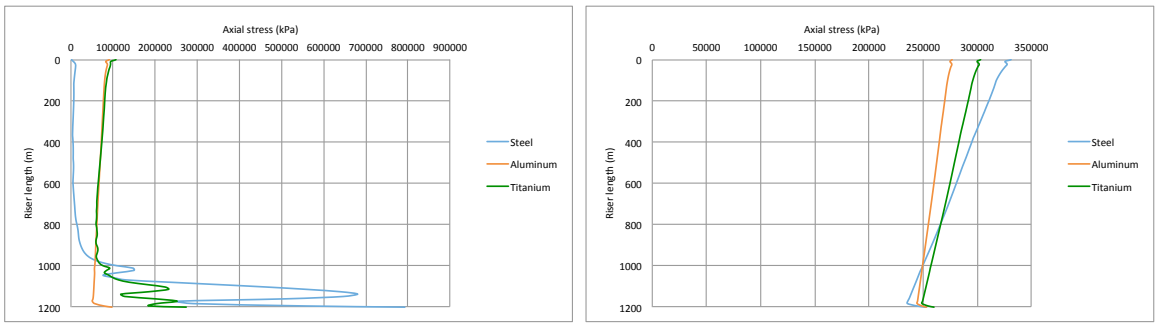

(a) 450 kN **(b)** 1950 kN

Fig. A.13. Max.Axial stress through the entire length of riser, drilling fluid density = $1500kg/m^3$